Research Square

Preprints are preliminary reports that have not undergone peer review.
They should not be considered conclusive, used to inform clinical practice,
or referenced by the media as validated information.

GPCR activation mechanisms across classes and macro/microscales

David Gloriam (david.gloriam@sund.ku.dk)
University of Copenhagen https://orcid.org/0000-0002-4299-7561
Alexander Hauser
University of Copenhagen
Albert Kooistra
University of Copenhagen https://orcid.org/0000-0001-5514-6021
Christian Munk
University of Copenhagen
M. Madan Babu
St. Jude Children's Research Hospital

Article

Keywords: Endogenous Ligands, Extracellular Binding, Microswitch Residue Positions, Molecular Mechanistic Maps, Functional Determinants, Conformational Selection, Allosteric Communication

Posted Date: April 1st, 2021

DOI: https://doi.org/10.21203/rs.3.rs-354879/v1

License: This work is licensed under a Creative Commons Attribution 4.0 International License.
Read Full License

Version of Record: A version of this preprint was published at Nature Structural & Molecular Biology on November 10th, 2021. See the published version at https://doi.org/10.1038/s41594-021-00674-7.

GPCR activation mechanisms across classes and macro/microscales

Alexander S. Hauser[1,4], Albert J. Kooistra[1,4], Christian Munk[3], M. Madan Babu[2] and David E. Gloriam[1*]

[1]*Department of Drug Design and Pharmacology, University of Copenhagen, Universitetsparken 2, 2100 Copenhagen, Denmark.*

[2]*Department of Structural Biology and Center for Data Driven Discovery, St. Jude Children's Research Hospital, Memphis, TN, USA.*

[3]*Present address: Novozymes A/S, Biologiens Vej 2, 2800 Kongens Lyngby Copenhagen, Denmark*

[4]*These authors contributed equally*

**Correspondence: david.gloriam@sund.ku.dk (D.E.G.)*

Two-thirds of human hormones and one-third of clinical drugs activate ~350 G protein-coupled receptors belonging to four classes: A, B1, C and F. Whereas a model of activation has been described for class A, very little is known about the activation of the other classes which differ by being activated by endogenous ligands bound mainly or entirely extracellularly. Here, we show that although they use the same structural scaffold and share several helix macroswitches, the GPCR classes differ in their microswitch residue positions and contacts. We present molecular mechanistic maps of activation for each GPCR class and new methods for contact analysis applicable for any functional determinants. This is the first superfamily residue-level rationale for conformational selection and allosteric communication by ligands and G proteins laying the foundation for receptor-function studies and drugs with the desired modality.

G protein-coupled receptors (GPCRs) are nature's primary transmembrane transducers for carrying signals from extracellular ligands to intracellular effectors to regulate numerous physiological processes. The most widely used nomenclature designates GPCR classes A-F and was introduced in the first version of the GPCR database, GPCRdb[1] based on conserved sequence fingerprints[2,3]. The human GPCRs have also been classified based on phylogenetic analysis into families (class): Glutamate (C), Rhodopsin (A), Adhesion (B2), Frizzled (F), Secretin (B1)[4] and Taste 2 (T, re-classified as a separate family in[5]). The human GPCRs are activated from different endogenous ligand binding sites in the transmembrane (class A) or extracellular domain (class C) or both (class B and F) and have very low sequence similarity (cross-class pairs mean 23%). This raises the question to what extent the GPCR superfamily utilises universal or unique activation mechanism. Considering that GPCRs mediate the actions of two-thirds of endogenous hormones and neurotransmitters[6] and over one-third of the drugs[7-9], mapping their activation mechanisms is important to understand human physiology, disease aetiology and to rationally design drug.

Comparison of inactive and active structures of class A GPCRs have uncovered common activation mechanisms within the seven transmembrane helices (7TM) that have been shown to tilt, rotate, elongate or switch residue sidechain rotamers to create contact networks stabilising the receptors in a specific state[10-13]. These contacts converge near the G protein site[14] and are conserved regardless of the subtypes of intracellular effectors[11]. Site-directed mutagenesis of contact residues has revealed differences in pharmacological responses, including constitutive activity[11] and signalling bias[15], and naturally occurring mutations have been associated with disease or change of response[11,16,17]. However, the classes B, C and F are largely unexplored with respect to common activation mechanisms and until now such studies have not been possible due to a lack of structures across the activation states.

In this work, we conducted a comprehensive comparative structural analysis of inactive/active state structures in each GPCR class by analysing all available 488 structures from different GPCR classes (Fig. 1). We present the first, GPCR superfamily-wide molecular mechanistic maps of activation and link determinants to ligand binding, G protein coupling, transduction and allosteric sites. This can serve as a roadmap to assess the

activation of any GPCR and to understand how common or distinct determinants can fine-tune physiological signalling responses and contribute to a desired drug efficacy.

Results

New dataset and methods for comparative structure analysis

To present the best maps possible to date, we made a comprehensive annotation of all available 406 structures of 74 class A GPCRs (twice as many as in any previous report[11]). These were applied to stringent quality filters to select the representative inactive/active state structures from each class (Methods and Supplementary Spreadsheet 1). Out of 68 templates used, 45 have a resolution of 3.0 Å or better. It should be noted, that in lower resolution structures (>3.0Å) mainly backbone movements can be discerned while residue contacts can only be underrepresented (i.e., not lead to false positive contacts). The largest number of structures belong to classes A and B1 and cover 22 out of 58 and all five receptor families (share endogenous ligand), respectively. This diversity ensures that any artefacts observed in a specific position or structure will only have a marginal effect on the overall frequency of movements and contacts.

We introduce a definition of state-specific contacts based on their relative frequency (%) in a given inactive/ active state. Like the scores calculated in[11], this allows for the identification of many more determinants than requiring 100% presence and absence, respectively in opposite states, such as the four inactive- and two active-state stabilising contacts identified in the first landmark study comparing five class A GPCRs across the states[14]. Importantly, the use of frequencies with (different) sets of inactive and active state structures opens up for the utilisation of also different receptors across the states, as the same helix backbone movements and contacts can be mediated by different amino acids. This is critical to the identification of a comparable number of state determinant residues in classes C and F for which the structural coverage is so far limited: four and three receptors, representing 18% and 27% of all members of these relatively small classes, respectively. Furthermore, we uniquely apply residue pair conservation cut-offs (Methods). Together, the combined contact

frequencies and conservation cut-offs address the class-representativeness allowing analyses across the GPCR superfamily.

GPCR activation engages all transmembrane helices with unique contact patterns

To investigate how the seven transmembrane helices, TM1-7 rearrange upon activation, we compared the 13 GPCRs among our representative receptors for which both an inactive and active state structure are available (Extended Data Table 1 and Methods). We find that each transmembrane helix rearranges >1.0 Å in a majority of receptors –demonstrating unappreciated conformational dynamics (class consensus is red in Fig. 2, individual receptor plots in Supplementary Figs. 1-2). Notably, the extracellular region alone exhibits a relocation of all seven transmembrane helices in class B1 wherein the N-terminal domain restricts the conformation the 7TM before activation[18]. GLP-1, which is the best template having a full-length inactive structure[18]), has a 2.5-10 Å relocation of TM1-7 – all of which also move in CRF1. Furthermore, we analysed the conformational change of each class across the mid, extracellular and cytosolic regions where the rearrangements total 6 Å, 12 Å and 28 Å and involving 24%, 45% and 65% of receptor helices. This is the first quantitated characterisation of magnitude and abundance of helix rearrangements at the mid, extracellular and cytosolic regions of the transmembrane domain. It supports opposite functional roles in i) maintaining a stable GPCR fold, ii) adapting to ligands of diverse sizes or iii) coupling to the much larger G proteins, respectively. This connects structure-function and reveals a wide engagement of the GPCR fold – across its helices and domains.

We next investigated how the rearrangements of the transmembrane helix bundle change the residue contact networks between receptor segments by comparing all 43 inactive and 25 active state representative structures (Extended Data Table 1). We find that in addition to TM1-7, state-specific contacts are also formed to helix 8 (H8) in classes A and F, intracellular loop 1 (ICL1) in class C and extracellular loop 2 (ECL2) in class F (Figs. 3-4). Classes A, C and F have a majority of inactivating contacts (66%, 56% and 62%, respectively, Fig. 3a). Of note, each contact typically spans a majority and at least 30% of all receptors in each class based on residue-residue conservation (Methods). Class B1 has 48% inactivating contacts spanning segment contacts (excluding

four intra-helix contacts). This characterisation of contacts by state – where the majority, or close to half for B1, of contacts restrain receptors into an inactive conformation – provides a structural rationale to why most receptors have no or little activity without the prior stimulation by an agonist. Furthermore, it demonstrates that any TM helices can switch from mainly inactive to active state contacts (Figure 3B). Notably, this rewiring leads to markedly different patterns of segment contacts across GPCR classes that combine several unique and some common contacts (below), as even high-homology receptors sharing endogenous ligand, such as the A_1 and A_{2A} adenosine or muscarinic acetylcholine M_1 and M_2 receptors, display unique helix movements (Fig. 2).

Together, the existence of both common and unique movements and contacts (below) provides a structural rationale for shared overall functions throughout the GPCR superfamily, e.g. ligand-dependent activation, signal transduction across the cell membrane and G protein coupling, that yet are diversified with respect to the specific ligand scaffold, G protein profile and functional response kinetics and efficacy.

TM6 is a universal helix 'macroswitch' but toggles, rotates and unwinds differently across GPCR classes

We next single helix rearrangements across 13 receptor inactive/active state structure pairs confirms. We find that outward movement and rotation of TM6 on the cytosolic side – opening for G protein coupling – is a universal feature of activation throughout the GPCR superfamily (Fig. 2a), as first suggested for class A[19]. Intracellular TM6 movement is observed in all 13 investigated receptors and is the largest in classes A (7-13 Å), B1 (14-19 Å) and F (7 Å) where is combined with a substantial average rotation: 38°, 39° and 38°, respectively. The opposite, extracellular end of TM6 also moves by on average 2.0, 3.4 and 6.2 Å, respectively, in these classes. The movement of TM6 gives it the largest (B1 and F) or second largest (A) number of contacts stabilising an inactive or active state in these classes (Fig. 3). However, our analysis shows that TM6 also displays large mechanistic differences across all the classes. Class B1 has a unique unwinding of the extracellular-facing half of TM6 in all three activated receptors[20-22]. This is in agreement with a recent study, comparing the class B1 Glucagon and class A β_2 receptors, linking the weaker ability of the agonist to induce the outward movement of cytoplasmic TM6 to a slower G protein activation[21]. Furthermore, in class C, TM6

uniquely has no extracellular movement and only a small (2.8 Å) movement and rotation (13°). Consequently, TM6 has only one state-specific contacts to other helices whereas TM5 has five and TM7, with two such contacts, is the only switch region with contacts across both states (Fig. 3b). The smaller role of TM6 in the activation throughout the class is supported by a markedly lower conservation of its proline, 55% compared to 93-100% in other classes A-C while the importance of TM7 is emphasised by a 95% conserved proline (Fig. 2b). The non-canonical small TM6 tilt with a less conserved kink and atypical contacts to the adjacent TM5 and TM7 are associated with a different overall mechanism, as class C GPCRs work as an asymmetric homo- or hetero-dimer in which only one of two subunits couples to a G protein.

These findings show that the GPCR activation machinery utilises TM6 as universal yet differentiated switches – combining helix toggling, rotation and unwinding. Such commonality across classes in the activation mechanism at the level of transmembrane helices but diversity and nuances at the type of movements provides an important structural rationale for drug discovery and in the future design of experiments to elucidate effects of mutations, ligand efficacy and G protein selectivity[23] mechanisms.

TM5 is a new universal switch, TM5-7 act in concert and TM3 is a hub for stabilisation of inactive or active receptors

TM5, like TM6, can be considered a universal switch for GPCR activation, as it moves on the intracellular side in all four classes (with on average A: 2.1, B1: 2.4, C: 2.0 and F: 1.8 Å), including a majority of class A and all class B1, C and F receptors (Fig. 2b and (Extended Data Fig. 2). TM7 also moves in all classes except class C, either on the cytosolic side (all class A receptors), the extracellular side (e.g. 10 Å movement and 100° rotation in GLP-1, the class B1 receptor with full-length templates) or on both sides (class F). These movements are possible due to a number of conserved proline and glycine residues that induce helix plasticity (Fig. 2b). Class A GPCRs have triple proline kinks in TM5-7, that allow TM5 and TM7 to close-in on and stabilise TM6. Class B1 TM6 unwinding is facilitated by both a proline kink (P6x47) and a glycine (G6x50). Class B1 GPCRs also feature a proline kink (P5x42) near the extracellular end of TM5, which moves 3.3 Å in GLP-1, and a glycine kink (G7x50) in TM7. Class F combines the TM6 switch with movements of cytosolic

TM5 (with one Pro and two Gly residues) and TM7 on both sides. This demonstrates that TM6 does not act on its own but is supported by TM5 and TM7 in a concerted movement and that the determinants of this plasticity are conserved throughout the classes.

We find that TM3 contacts the largest number (3-5) other receptor segments in each GPCR class (Fig. 3), revealing that TM3 functions as a stabilisation hub – not just to maintain the common transmembrane fold[24] – but to stabilise a specific inactive or active state across the GPCR superfamily. Furthermore, whereas an early report based on two class A GPCRs suggested an activation mechanism involving an upward movement of TM3[25], our analysis of TM helix movements in 15 receptors across classes instead points to rotation as the main mechanism (Extended Data Fig. 1). In 11 out of 13 the investigated receptor pairs (all except A_{2A} and CRF1), TM3 rotates at either the cytosolic (most frequent for class A, average 16°) or extracellular end (classes B1, C and F, average 19°, 12° and 17°, respectively) – while no receptor rotates in both ends or in the mid (Figs. S1-2). Lateral movement of TM3 contributes to a different extent across classes spanning from both ends (B1), cytosolic end (C), either end for a minority of receptors (A) to no movement (F). In contrast, TM4 – which is peripherally located in the transmembrane helix bundle – has few or no contacts (class A:1, B1:0, C:3 and F:0). This shows that the abundant helix packing has not immobilised TM3 which instead, by an array of mainly local rotation or movement, contributes to GPCR activation in several places.

Contact state frequency approach uncovers residue 'microswitches' in all GPCR classes and expands class A activation model

To investigate state determinants on the residue 'microswitch' level, we indexed topologically corresponding receptor positions with generic residue numbers[26] and classified them into 'inactivators', 'activators' and 'switches' based on frequent contacts in inactive, active and both states, respectively (Methods). We uncover a comparable number of state determinants across classes: A: 41, B1: 33, C: 28 and F: 33 (Fig. 4). 86% of determinants (A: 80%, B1: 72%, C: 100% and F: 91%) are inactivators or activators whereas only 16 determinants are switches. Only 9 switches undergo sidechain rotamer shifts (residue text rotation in Fig. 4a) revealing that that the rotamer microswitches – described as major state determinants for class A GPCRs[12,13]

– play a small role in the GPCR superfamily. Importantly, many determinant positions contain the same highly conserved amino acid (grey scaling in Fig. 4a) and the amino acid pairs observed for each contact are conserved in at least 40% of all receptors (Methods). Notably, this includes the reference positions for generic residue numbers (index x50) in 5 out of 7 transmembrane helices, helix 8 and ICL1 and all major previously known class A state determinants (sequence motifs and microswitches with magenta border in Fig. 4a)[11,12]. This demonstrates that our new approach (Discussion) identifies both known and new conserved determinants – even where the structural coverage is so far limited including the active state of classes C and F.

In class A, W6x48, initially described as a rotamer toggle switch[12] does not itself undergo a rotamer but a helix rotational shift (of 10°) and is approached by I3x40 which has both types of rotations. This provides an alternative to a reported 'PIF' motif[27-29] which is here found to consist most frequently of 'PIW' (P5x50 being the third residue). The PIFs motifs last residue, F6x44 is instead here shown to act as a switch in another new triplet 'LLF' located on the same helices: TM3, TM5 and TM6. The two residues D2x50 and N7x49 which coordinate a sodium ion[30] are here found to have a direct interaction stabilising the inactive state. Notably, N7x49 contacts P7x50 uncovering a concerted stabilisation across the sodium ion site and TM7 helix kink around the 'NPxxY' motif. The final residue of the NPxxY motif, a Y7x53 switch[11-13], has three inactivating and two activating state-specific contacts with over 40% frequency difference, including to another switch: I3x46. The TM3 'DRY' motif includes an intra-helical ionic lock from D3x49 to R3x50, which upon activation swings to interact with the G protein as well as the switch Y5x58 on TM5. Of note, the restraining of R3x50 is strengthened by contacts to TM2 and TM6 (A6x34) – however typically not to E6x30, which was part of the first ionic lock reported in Rhodopsin[31] but less conserved (E: 25% or D/E: 31% compared to D: 65% or D/E: 86% for position 4x49). On the intracellular side, helix 8 and ICL1 contain three and two determinants, respectively, including the novel switch F8x50 contacting another new switch on TM7, A7x54. These findings corroborate the findings of previous studies on class A[10-14]. They also, together with the concerted movement of TM5-7 and role of TM3 as a state stabilisation hub (above), substantially expand the activation model of class A receptors – the largest class of GPCRs in human.

Class B1 shares many class A state determinant residues while having a unique concentration in and around the TM6 helix switch

The first comparison of unique and common state determinants across the GPCR superfamily shows that nearly half, 16 out of 33, of the B1 determinants maps to equivalent topological positions as in class A compared to 10 for class F and 8 for class C (leftmost in Fig. 4b). Furthermore, the classes B1 and A have four common switches (second to rightmost in Fig. 4b). Notably, this includes the two known microswitches (A/B1 residue number): Y5x58/F5x54 and Y7x53/Y7x57 as well as the pair I3x46/E3x50 and F6x44/L6x49 (magenta in Extended Data Fig. 3). We also find that the class A 'toggle switch' activator W6x48 is also conserved in class B1 as a smaller aromatic residue Y6x53 (Extended Data Fig. 3). Together, these commonalities between classes B1 and A are indicative of an, in part, shared activation mechanism.

However, there are also markedly unique features in class B1. Strikingly, 14 out of 33 of state determinants in class B1 are clustered on one helix, TM6 which engages 10 additional determinants – of which all except one are located in TM5 and TM7 (Fig. 4) which move together with TM6 (Fig. 2). The high concentration of state determinants in TM6 and packing to adjacent helices, may provide a plausible structural rationale for a recent report demonstrating a higher energy barrier for the formation of the kinked and partially unwound TM6 in the class B1 Glucagon receptor compared to the class A β_2-adrenoceptor[21]. Another unique feature in class B1 are two additional switches on TM7 (Q7x49 and L7x56). Class B1, like class A, has a large structural coverage (10 out of 15 receptors) and contains several major drug targets[7]. The first map of state determinants in class B1 gives a better understanding of the basic receptor activation mechanisms and presents a foundation for the targeting of determinant networks in structure-based design of new drugs stabilising receptors in desired states.

The GPCR superfamily lacks a universal residue-level microswitch mechanism

Class C is atypical in that it contains as many inactivating and activating contacts and no switches in the transmembrane domain (compared to 3-8 in the other classes, two-way Venn diagram in Fig. 4a). This is in concordance with its – by far – smallest conformational change (Fig. 2). Another characteristic of class C is

that it has the highest share of determinants, 36% (compared to A: 20%, B1: 24% and F: 0%) that form contacts within the same transmembrane helix. As class C is the only GPCR class that binds endogenous ligands entirely in the N-terminus, the transmembrane domain solely transduces signals. On the cytosolic side this involves two determinants in ICL1 (as in class A). Class F uniquely has frequent state stabilising contacts to ECL2, Y45x51 and V45x52 – both of which stabilise the active state by interaction with the same residue, F3x29 in TM3. The two ECL2 positions follow a conserved cysteine C45x50 which forms a covalent disulphide bridge, also to TM3, across the GPCR classes[32]. Class F has the highest conservation of determinant consensus amino acids (on average 90.5%) showing that the vast majority of contacts identified in the three structural templates: FZD4, FZD5 and Smoothened are likely shared by its remaining eight receptors. Class F has three switches, M3x37, W3x50 and M6x30 of which the former two have a large sidechain rotamer shift (49° and 47°, respectively). Interestingly, like class A, class F has a switch in position 3x50 although occupied by a trypthophan (A has arginine).

By comparing all GPCR classes, we find that 57 out of 91 determinant positions reside in a distinct topological position and are therefore unique, whereas 25 are found in two classes, 8 in three classes and only 1 throughout the GPCR superfamily (leftmost Venn in Fig. 4b). Of note, the universal determinant position (numbered 3x46 in class A/F and 3x50 in class B1/C) plays a different role as inactivator (C), activator (F) or switch (A/B1). Considering such different roles in all determinant positions reveals an even smaller commonality – presence in a maximum of two GPCR classes for 12 inactivators (max 4 in A-F), 5 activators (max 2 in A-B1 and B1-F) and 5 switches (max 4 A-B1) (second to rightmost Venn in Fig. 4b and Extended Data Fig. 3). These findings demonstrate that although they belong to the same superfamily, use the same structural scaffold and share several macroswitches (helices), the GPCR classes differ in their microswitches (residues). This suggests that there are an ensemble of structural/mechanistic solutions that is available for the GPCR superfamily during evolution that different receptor classes have explored and utilised. It also means that while thinking about developing drugs with different modalities – especially for classes C and F – one should aim to interact with

or modulate class specific state determinants and residue-level micro-switches rather than use the same state determinant and switch as in class A.

State determinant mapping reveals where ligands and G proteins can sense and stabilise receptor states

To obtain a topological and functional mapping of the state determinants, we mapped their location in relation to 408 ligand and 125 Gα protein interacting positions across the GPCR classes (grey and orange in Fig. 5) extracted from all 488 available GPCR structures. We find that all GPCR classes have the largest share, 60-68% of state determinants in ligand binding positions (Supplementary Spreadsheet 2). Class B1 is the only GPCR class with an even share across orthosteric and allosteric ligand positions (above/below membrane "Mid" in hexagon residue on TM1-7). Class A has only three (2%) determinants (W6x48, L7x40 and S7x46) in orthosteric ligand-binding positions and other state stabilisers are located below the membrane mid. Whereas class F has 18% of such determinants, class C lack orthosteric determinants altogether in the 7TM, as it binds its endogenous ligands solely in the N-terminus. When instead considering the proportion of state determinants in G protein binding positions, we find that these account for around one-third in classes A (29%) and B1 (36%) but a much smaller fraction in classes C and F (6-7%). For class C this may reflect its uniquely shallow G protein binding but the figures in both classes is likely underrepresented due to few G protein complex structures. The remaining determinants (at non-interacting positions) account for 21-36% on the GPCR class level.

Given their important role in modulating GPCR activity, we made a specific mapping of switches i.e. determinant residues that alternate contacts across the inactive/active states. In class A, two switches (R3x50 and 5x58) have direct G protein interactions whereas the remaining six are located near or in between ligand and G protein positions facilitating the allosteric signal transduction across the extra- and intra-cellular sides. Class B1 switches are distributed across orthosteric ligand (6x49), G protein (3x50, 7x56 and 7x57) and two other (5x54 and 7x49) positions. Class C uniquely has no switches in the transmembrane domain. Finally, class F shares one class A switch with G protein interaction (3x50) and has two switches in positions without

a known interaction. Together, this functional mapping shows that ligands and G proteins can sense and stabilise receptor states by direct interactions and that their signals are largely transduced via interconnecting pathways while state determinants including switches are spread throughout the 7TM bundle. This may help to explain observed effects on ligand or G protein affinity from remote mutations and presents a residue-level rationale for conformational selection[33] and allosteric modulation[34].

Discussion

We present the first molecular mechanistic maps for activation across the GPCR superfamily and helix macro-/residue micro-scales while extending beyond the transmembrane region to helix 8 and structurally conserved loop segments. This study has answered the fundamental question of whether the activation of other classes can be modelled based on class A – they cannot. Our findings demonstrate that although they belong to the same superfamily, use the same structural scaffold and share several helix macroswitches, the GPCR classes differ in their microswitch residue positions, contacts and amino acids. This applies also to class B1 which shares about half of the determinant positions in class A, as the similarity is very small if considering the type of determinant – stabilising an inactive, active or both states – and their specific consensus amino acids. This highlights the need to elucidate each GPCR class' restraints and diverse activation mechanisms separately and in more detail to adequately capture structure-function relationships. Determinants of receptor activity are tightly tied to the molecular mechanisms of conformational selection (Kenakin, 2019) and allosteric modulation[34], and influence an array of functions and responses, including ligand affinity, basal activity, efficacy and G protein coupling. Therefore, the contact maps (Fig. 4) presented here provide an actionable foundation for the field to design and interpretate experiments across structural, biophysics (e.g. fluorescence and double electron-electron resonance), molecular dynamics and mutagenesis studies. The maps also inform drug discovery of which inactivating and activating state determinants are located in the orthosteric and allosteric ligand sites and may therefore facilitating effective design of inverse agonists, neutral antagonists or agonists for different receptors.

The extensive engineering and limited resolution of some structures is an inherent limitation for all structure-based studies. Therefore, more structures and advances in their determination are of outmost value and will serve to continuously refine structure-function relationships generally. For example, the universal TM5 switch reported herein was not discernible until cryo-electron microscopy allowed for more structures with a native TM5-ICL3-TM6 region (often subjected to deletion and protein fusion in crystallography fusions not in cryo-EM). Our combined contact frequency and residue pair conservation cut-offs uniquely addresses the class-representativeness and allowed for the GPCR superfamily to be described. Class F has a 90.5% average conservation of determinant consensus amino acids. For these reasons, the common conserved determinants identified herein should still apply as our knowledge expands from new structures, which could also allow additional determinants fulfil these cut-offs. Furthermore, although specific receptors and subsets thereof could have additional activation mechanisms not conserved in the whole class, and such specific and general mechanisms, respectively could act in concert.

Acknowledgements

This work was supported by the Lundbeck Foundation (grants R163-2013-16327 and R218-2016-1266), the Novo Nordisk Foundation (grant NNF18OC0031226) and Independent Research Fund Denmark | Natural Sciences (grant 8021-00173B) to D.E.G and by the American Lebanese Syrian Associated Charities (ALSAC). to M.M.B.

Author Contributions

Conceptualization, D.E.G.; Methodology, D.E.G., C.M. and A.J.K.; Data Curation, A.J.K.; Investigation, D.E.G.; Validation: D.E.G. and A.J.K.; Writing – Original Draft, D.E.G.; Writing – Review & Editing, A.S.H. and M.M.B.; Visualization, D.E.G., A.S.H. and A.J.K., Funding Acquisition, D.E.G. and M.M.B.; Supervision, D.E.G.

Competing interests

The authors declare no competing interests.

Online content

Methods, additional references, Nature Research reporting summaries, source data, extended data, peer review information; and statements of data and code availability are available at [URL].

Main figures

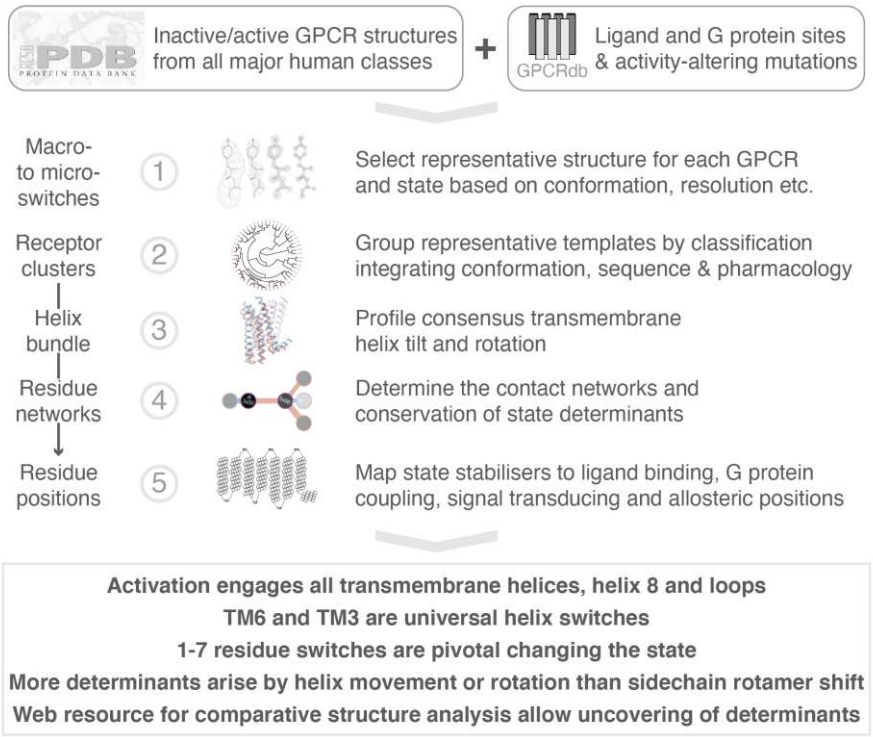

Fig. 1 | Analysis pipeline for elucidation of GPCR activation mechanisms. Pipeline for analysis of universal and distinct activation macro-/microswitches spanning helix repacking to sidechain rotation and connection to ligand binding, G protein coupling and signal transduction sites (see Methods).

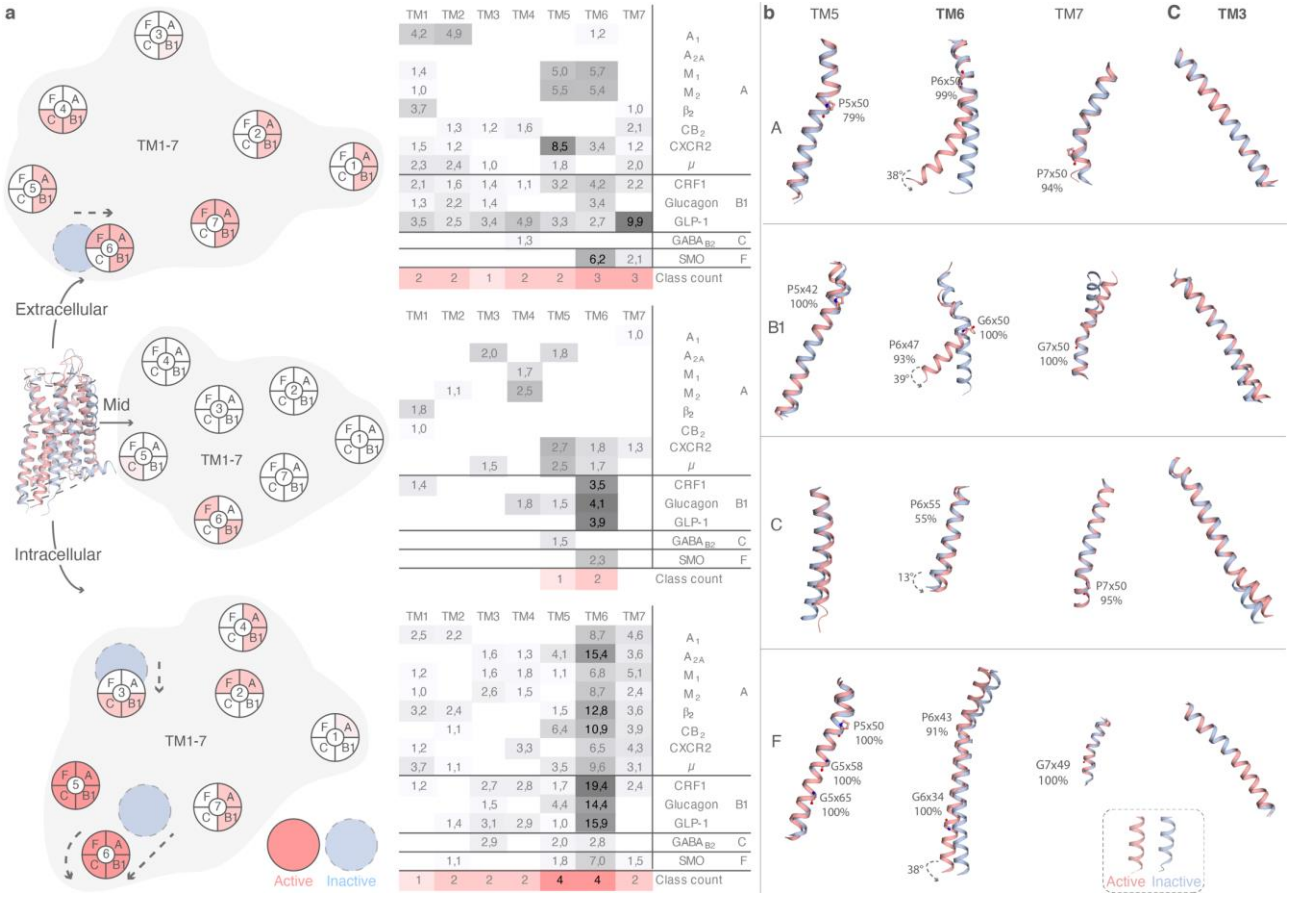

Fig. 2 | Transmembrane helix movement upon activation and universal TM3 and TM6 helix 'macroswitches'. a, Movements (Å) over 1.0 Å at the extracellular end, membrane mid (determined using[35]) and intracellular end of the transmembrane helices, TM1-7 upon comparison of all available receptor inactive- and active-state structure pairs (Extended Data Table 1). Red intensity denotes the number of classes with a consensus movement (for class C, priority is given to the Gi-$GABA_{B2}$ over the non-coupled mGluR5 structure). **b**, Movement and conserved hinges of TM6 and the adjacent TM5 and TM7. **c**, TM3 cytosolic tilt and overall rotation. **b-c**, GPCR class representative inactive/active receptor structure pairs: A: β_2[36,37], B1: GLP-1[18,22], C: $GABA_{B2}$[38] and F: Smoothened[39,40] receptors. Proline and glycine residues that increase helix plasticity are shown along with their percent conservation in the GPCR class.

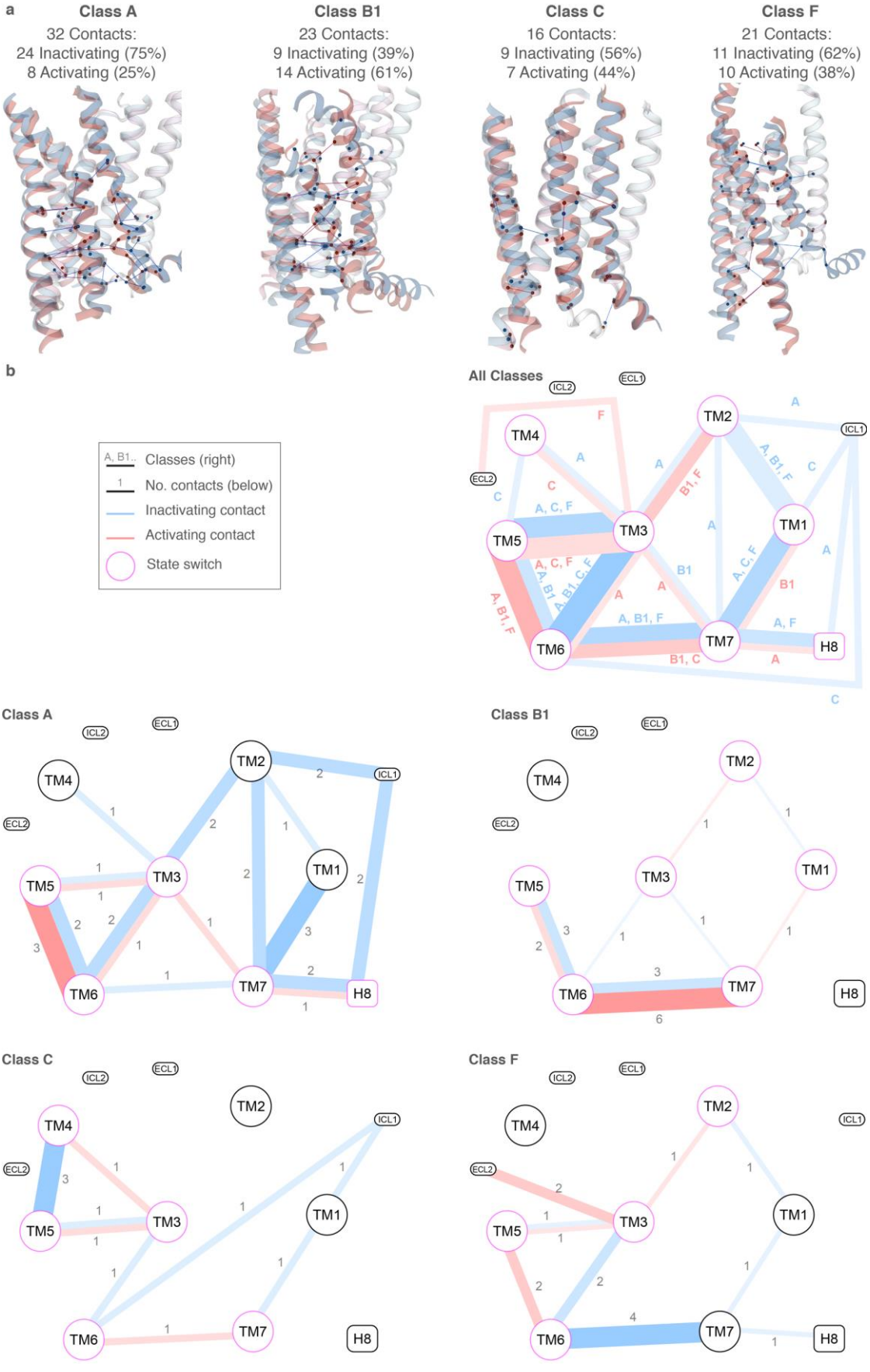
a
Class A
32 Contacts:
24 Inactivating (75%)
8 Activating (25%)
Class B1
23 Contacts:
9 Inactivating (39%)
14 Activating (61%)
Class C
16 Contacts:
9 Inactivating (56%)
7 Activating (44%)
Class F
21 Contacts:
11 Inactivating (62%)
10 Activating (38%)
b
A, B1..
Classes (right)
1
No. contacts (below)
Inactivating contact
Activating contact
State switch
All Classes
Class A
Class B1
Class C
Class F
ICL2
ECL1
ECL2
ICL1
TM1
TM2
TM3
TM4
TM5
TM6
TM7
H8

Fig. 3 | GPCR stabilise inactive and active states by rerouting contacts between TM1-7, H8, ICL1 and ECL2. a, State-specific residue-residue contacts in each GPCR class visualised as lines within representative inactive/active receptor structure pairs (same as in Fig. 2b-c). Numbers indicate the total, inactivating and activating contacts in each GPCR class. **b**, Contact networks between the seven GPCR transmembrane helices, TM1-7 and the first intracellular (ICL1) and second extracellular (ECL2) loops (intra-segment contacts not shown). Line thickness represents the number of classes (topmost) or contact frequency differences between the inactive and active states. Line colour indicates inactivating (blue) and activating (red) contacts. Receptor segments with a magenta border are "switches", i.e. have contacts across both states. Contacts are identified based on a higher frequency (%) in one set of 43 inactive and 25 active state receptors. **a-b**, The frequency difference thresholds was set according to the structural coverage in each GPCR class' (no. members and inactive/active state templates): A: 40% (285, 33/14), B1: 67% (15, 3/10), C: 75% (22, 4/1) and F: 100% (11, 3/1) – yielding comparable numbers of determinants and contacts. To ensure that the identified determinants are applicable for throughout each class, we applied a cut-off requiring at least 30% of all its receptors to contain one of the amino acid pairs observed to form the given state specific contact. Contact definitions are explained in the settings menu of the online 'Comparative structure analysis' tool (https://review.gpcrdb.org/structure_comparison/comparative_analysis).

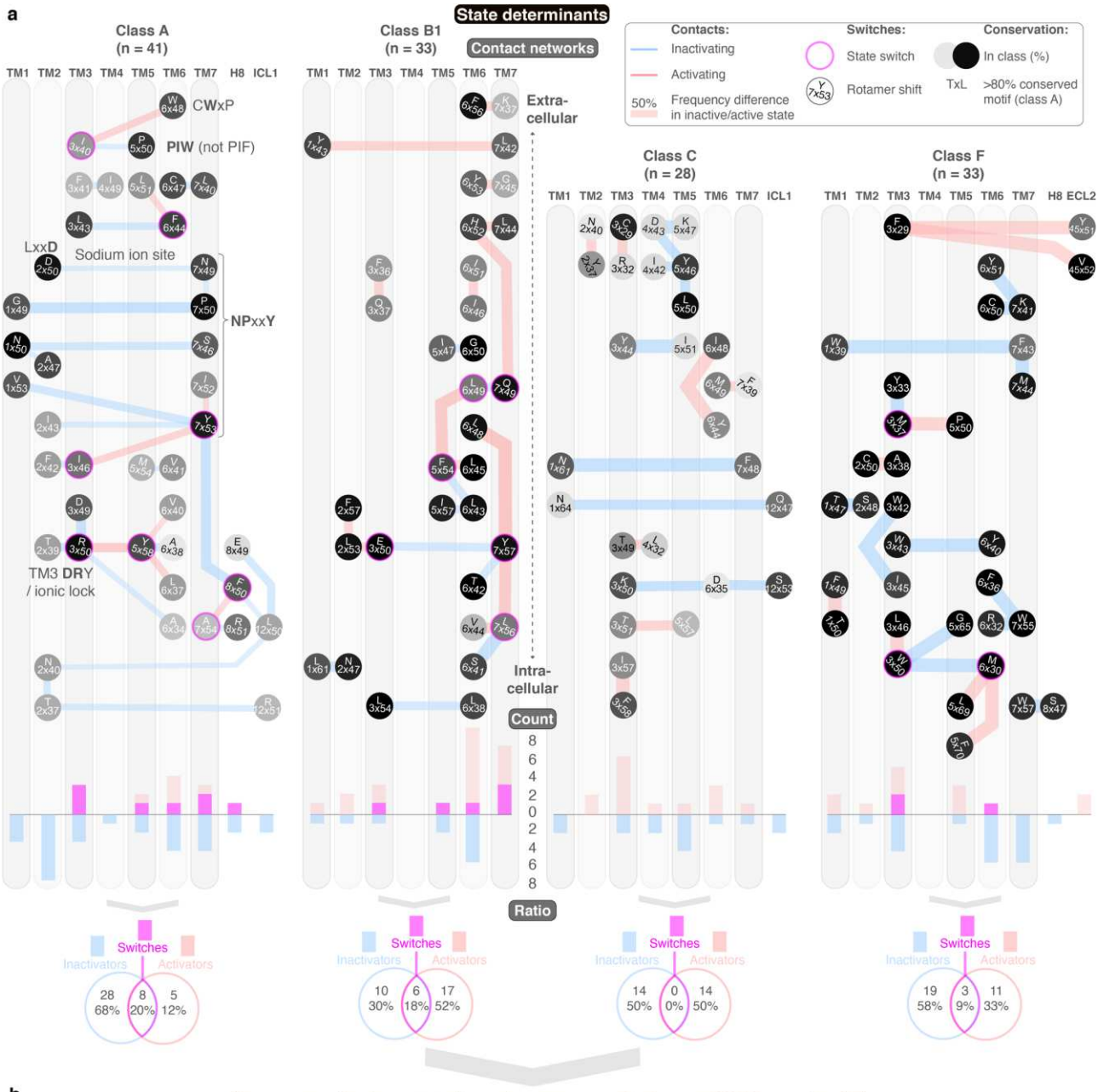
a
State determinants
Contact networks
Class A
(n = 41)
Class B1
(n = 33)
Class C
(n = 28)
Class F
(n = 33)
Contacts:
Inactivating
Activating
50%
Frequency difference
in inactive/active state
Switches:
State switch
Rotamer shift
Conservation:
In class (%)
TxL
>80% conserved
motif (class A)
CWxP
PIW (not PIF)
LxxD
Sodium ion site
NPxxY
TM3 DRY
/ ionic lock
Extra-
cellular
Intra-
cellular
Count
Ratio
Switches
Inactivators
Activators
28
68%
8
20%
5
12%
10
30%
6
18%
17
52%
14
50%
0
0%
14
50%
19
58%
3
9%
11
33%
b
Common and unique state determinants across the human GPCR superfamily
All state determinants
(n = 91)
Inactivators
(n = 58)
Switches
(n = 12)
Activators
(n = 43)
A
B1
C
F

Fig. 4 | State stabilising contact maps and differences at the residue-level 'microswitches'. a, Contact networks visualise the wiring of state determinants from the extracellular (top) to intracellular (bottom) sides. Contact frequency differences between the inactive and active states are shown as varied line thickness and residue rotamers as rotation of the consensus amino acid in analysed structures and its generic residue number. Two-way Venn diagrams depict the number and percentages of inactivator (blue), activator (red) and switch (magenta) state determinant positions. Bar diagrams show their distribution across the TM helices, H8 and loops. **b**, Comparison of common and unique state determinant positions across all investigated classes.

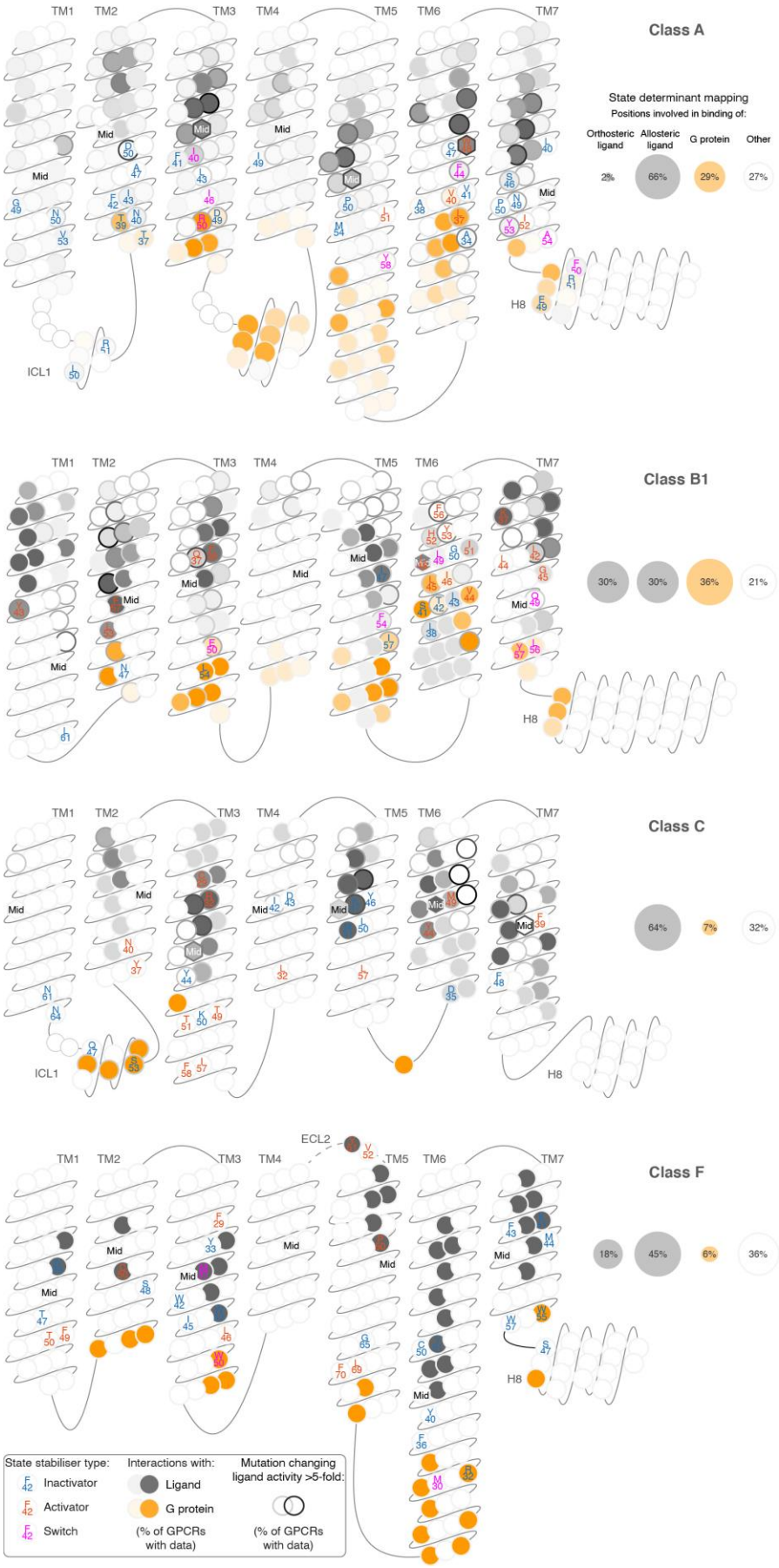
TM1
TM2
TM3
TM4
TM5
TM6
TM7
Class A
State determinant mapping
Positions involved in binding of:
Orthosteric ligand
Allosteric ligand
G protein
Other
2%
66%
29%
27%
ICL1
H8
Class B1
30%
30%
36%
21%
Class C
64%
7%
32%
ECL2
Class F
18%
45%
6%
36%
State stabiliser type:
Inactivator
Activator
Switch
Interactions with:
Ligand
G protein
(% of GPCRs with data)
Mutation changing ligand activity >5-fold:
(% of GPCRs with data)

1

Fig. 5 | Residue positions stabilising an inactive and/or active receptor state. GPCR snakeplots mapping the residue positions that form distinct contacts between state determinants classified as inactivators (blue), activators (red) and switches (magenta). Residues are denoted with the consensus amino acid of the investigated receptor structures (Extended Data Table 1) and their generic residue number[26]. Filled positions map ligand (grey) and G protein (orange) interaction frequency among all GPCRs in the given class that have such data (Supplementary Spreadsheet 2). Border grayscale denotes the frequency of mutations changing the ligand affinity or activity over 5-fold. The label "Mid" within hexagon-shaped positions denote the membrane mid, above and below which the ligand positions are considered orthosteric and allosteric, respectively, in class A, B1 and F. In class C, all ligand interacting positions in the seven transmembrane helices are allosteric, as its endogenous ligands bind solely in the N-terminal domain.

References

1 Kolakowski, L. F., Jr. GCRDb: a G-protein-coupled receptor database. *Recept Channels* **2**, 1-71994).

2 Attwood, T. K. & Findlay, J. B. Design of a discriminating fingerprint for G-protein-coupled receptors. *Protein Eng.* **6**, 167-176, doi:10.1093/protein/6.2.167 (1993).

3 Attwood, T. K. & Findlay, J. B. Fingerprinting G-protein-coupled receptors. *Protein Eng.* **7**, 195-203, doi:10.1093/protein/7.2.195 (1994).

4 Fredriksson, R., Lagerstrom, M. C., Lundin, L. G. & Schioth, H. B. The G-protein-coupled receptors in the human genome form five main families. Phylogenetic analysis, paralogon groups, and fingerprints. *Molecular pharmacology* **63**, 1256-1272, doi:10.1124/mol.63.6.1256 (2003).

5 Nordstrom, K. J., Sallman Almen, M., Edstam, M. M., Fredriksson, R. & Schioth, H. B. Independent HHsearch, Needleman--Wunsch-based, and motif analyses reveal the overall hierarchy for most of the G protein-coupled receptor families. *Mol Biol Evol* **28**, 2471-2480, doi:10.1093/molbev/msr061 (2011).

6 Foster, S. R. *et al.* Discovery of Human Signaling Systems: Pairing Peptides to G Protein-Coupled Receptors. *Cell* **179**, 895-908 e821, doi:10.1016/j.cell.2019.10.010 (2019).

7 Hauser, A. S., Attwood, M. M., Rask-Andersen, M., Schioth, H. B. & Gloriam, D. E. Trends in GPCR drug discovery: new agents, targets and indications. *Nat. Rev. Drug Discov.* **16**, 829-842, doi:10.1038/nrd.2017.178 (2017).

8 Sriram, K. & Insel, P. A. G Protein-Coupled Receptors as Targets for Approved Drugs: How Many Targets and How Many Drugs? *Molecular pharmacology* **93**, 251-258, doi:10.1124/mol.117.111062 (2018).

9 Santos, R. *et al.* A comprehensive map of molecular drug targets. *Nat. Rev. Drug Discov.* **16**, 19-34, doi:10.1038/nrd.2016.230 (2017).

10 Flock, T. *et al.* Selectivity determinants of GPCR-G-protein binding. *Nature* **545**, 317-322, doi:10.1038/nature22070 (2017).

11 Zhou, Q. *et al.* Common activation mechanism of class A GPCRs. *Elife* **8**, e50279, doi:10.7554/eLife.50279 (2019).

12 Nygaard, R., Frimurer, T. M., Holst, B., Rosenkilde, M. M. & Schwartz, T. W. Ligand binding and micro-switches in 7TM receptor structures. *Trends in pharmacological sciences* **30**, 249-259, doi:10.1016/j.tips.2009.02.006 (2009).

13 Carpenter, B. & Tate, C. G. Active state structures of G protein-coupled receptors highlight the similarities and differences in the G protein and arrestin coupling interfaces. *Current opinion in structural biology* **45**, 124-132, doi:10.1016/j.sbi.2017.04.010 (2017).

14 Venkatakrishnan, A. J. *et al.* Diverse activation pathways in class A GPCRs converge near the G-protein-coupling region. *Nature* **536**, 484-487, doi:10.1038/nature19107 (2016).

15 Schonegge, A. M. *et al.* Evolutionary action and structural basis of the allosteric switch controlling beta2AR functional selectivity. *Nat Commun* **8**, 2169, doi:10.1038/s41467-017-02257-x (2017).

16 Hauser, A. S. *et al.* Pharmacogenomics of GPCR Drug Targets. *Cell* **172**, 41-54 e19, doi:10.1016/j.cell.2017.11.033 (2018).

17 Schoneberg, T. & Liebscher, I. Mutations in G Protein-Coupled Receptors: Mechanisms, Pathophysiology and Potential Therapeutic Approaches. *Pharmacol. Rev.* **73**, 89-119, doi:10.1124/pharmrev.120.000011 (2021).

18 Wu, F. *et al.* Full-length human GLP-1 receptor structure without orthosteric ligands. *Nat Commun* **11**, 1272, doi:10.1038/s41467-020-14934-5 (2020).

19 Schoneberg, T., Schultz, G. & Gudermann, T. Structural basis of G protein-coupled receptor function. *Molecular and cellular endocrinology* **151**, 181-193, doi:10.1016/s0303-7207(99)00017-9 (1999).

20 Liang, Y. L. *et al.* Toward a Structural Understanding of Class B GPCR Peptide Binding and Activation. *Mol. Cell* **77**, 656-668 e655, doi:10.1016/j.molcel.2020.01.012 (2020).

21 Hilger, D. *et al.* Structural insights into differences in G protein activation by family A and family B GPCRs. *Science* **369**, eaba3373, doi:10.1126/science.aba3373 (2020).

22 Zhang, X. *et al.* Differential GLP-1R Binding and Activation by Peptide and Non-peptide Agonists. *Mol. Cell* **80**, 485-500 e487, doi:10.1016/j.molcel.2020.09.020 (2020).

23 Capper, M. J. & Wacker, D. How the ubiquitous GPCR receptor family selectively activates signalling pathways. *Nature* **558**, 529-530, doi:10.1038/d41586-018-05503-4 (2018).

24 Venkatakrishnan, A. J. *et al.* Molecular signatures of G-protein-coupled receptors. *Nature* **494**, 185-194, doi:10.1038/nature11896 (2013).

25 Tehan, B. G., Bortolato, A., Blaney, F. E., Weir, M. P. & Mason, J. S. Unifying family A GPCR theories of activation. *Pharmacology & therapeutics* **143**, 51-60, doi:10.1016/j.pharmthera.2014.02.004 (2014).

26 Isberg, V. *et al.* Generic GPCR residue numbers - aligning topology maps while minding the gaps. *Trends in pharmacological sciences* **36**, 22-31, doi:10.1016/j.tips.2014.11.001 (2015).

27 Rasmussen, S. G. *et al.* Structure of a nanobody-stabilized active state of the beta(2) adrenoceptor. *Nature* **469**, 175-180, doi:10.1038/nature09648 (2011).

28 Wacker, D. *et al.* Structural features for functional selectivity at serotonin receptors. *Science* **340**, 615-619, doi:10.1126/science.1232808 (2013).

29 Huang, W. *et al.* Structural insights into micro-opioid receptor activation. *Nature* **524**, 315-321, doi:10.1038/nature14886 (2015).

30 White, K. L. *et al.* Structural Connection between Activation Microswitch and Allosteric Sodium Site in GPCR Signaling. *Structure* **26**, 259-269 e255, doi:10.1016/j.str.2017.12.013 (2018).

31 Palczewski, K. *et al.* Crystal structure of rhodopsin: A G protein-coupled receptor. *Science* **289**, 739-745, doi:10.1126/science.289.5480.739 (2000).

32 de Graaf, C., Foata, N., Engkvist, O. & Rognan, D. Molecular modeling of the second extracellular loop of G-protein coupled receptors and its implication on structure-based virtual screening. *Proteins* **71**, 599-620, doi:10.1002/prot.21724 (2008).

33 Kenakin, T. Biased Receptor Signaling in Drug Discovery. *Pharmacol. Rev.* **71**, 267-315, doi:10.1124/pr.118.016790 (2019).

34 DeVree, B. T. *et al.* Allosteric coupling from G protein to the agonist-binding pocket in GPCRs. *Nature* **535**, 182-186, doi:10.1038/nature18324 (2016).

35 Lomize, M. A., Pogozheva, I. D., Joo, H., Mosberg, H. I. & Lomize, A. L. OPM database and PPM web server: resources for positioning of proteins in membranes. *Nucleic Acids Res.* **40**, D370-376, doi:10.1093/nar/gkr703 (2012).

36 Cherezov, V. *et al.* High-resolution crystal structure of an engineered human beta2-adrenergic G protein-coupled receptor. *Science* **318**, 1258-1265, doi:10.1126/science.1150577 (2007).

37 Rasmussen, S. G. *et al.* Crystal structure of the beta2 adrenergic receptor-Gs protein complex. *Nature* **477**, 549-555, doi:10.1038/nature10361 (2011).

38 Mao, C. *et al.* Cryo-EM structures of inactive and active GABAB receptor. *Cell Res.* **30**, 564-573, doi:10.1038/s41422-020-0350-5 (2020).

39 Wang, C. *et al.* Structure of the human smoothened receptor bound to an antitumour agent. *Nature* **497**, 338-343, doi:10.1038/nature12167 (2013).

40 Qi, X., Friedberg, L., De Bose-Boyd, R., Long, T. & Li, X. Sterols in an intramolecular channel of Smoothened mediate Hedgehog signaling. *Nat. Chem. Biol.* **16**, 1368-1375, doi:10.1038/s41589-020-0646-2 (2020).

Extended Data

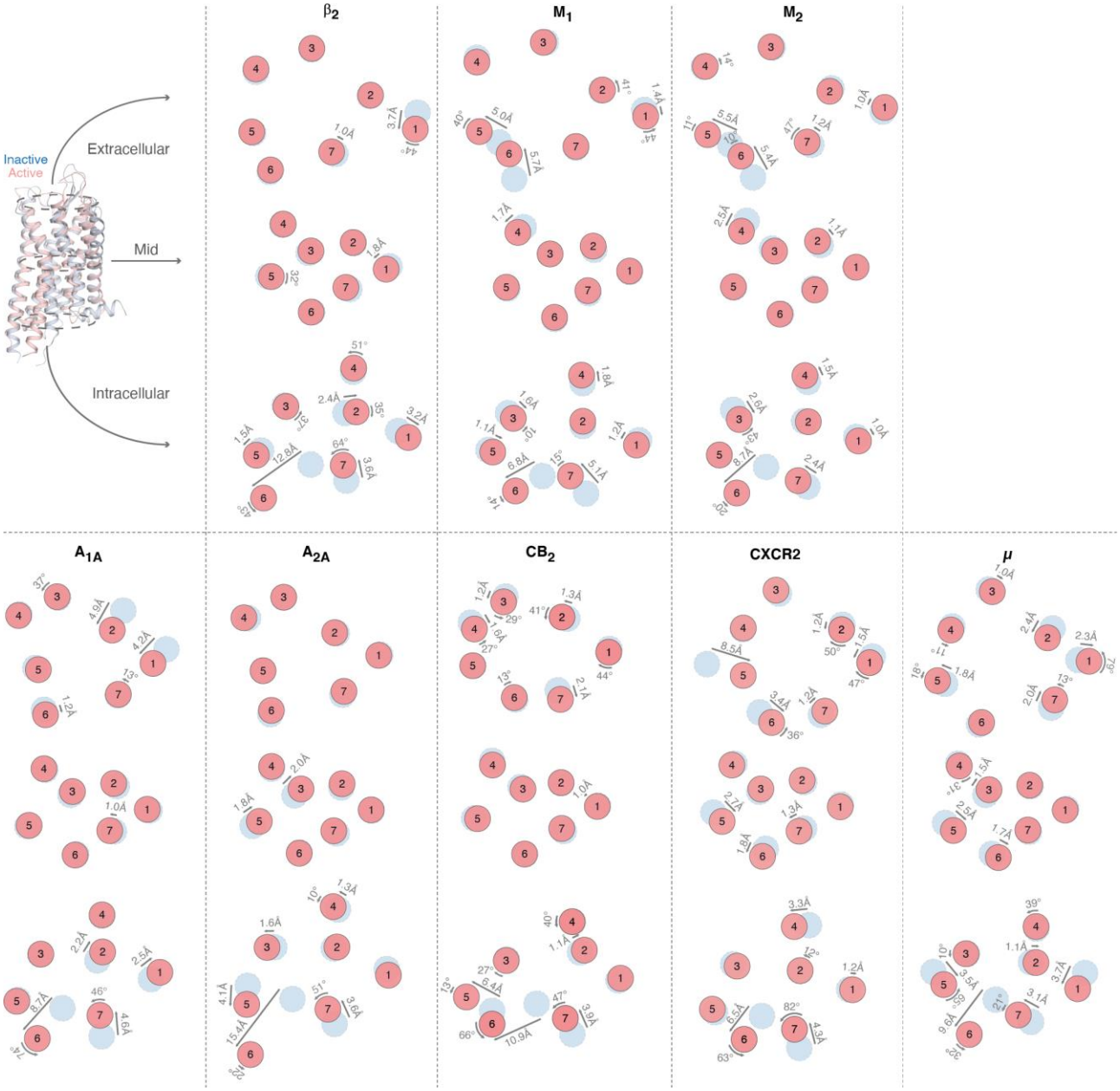

Extended Data Fig. 1 | TM1-7 movement of class A receptor pairs upon activation. Transmembrane helix movement at the extracellular face, membrane mid and intracellular face based on comparison of representative inactive and active state structure pairs of class A GPCRs (Extended Data Table 1).

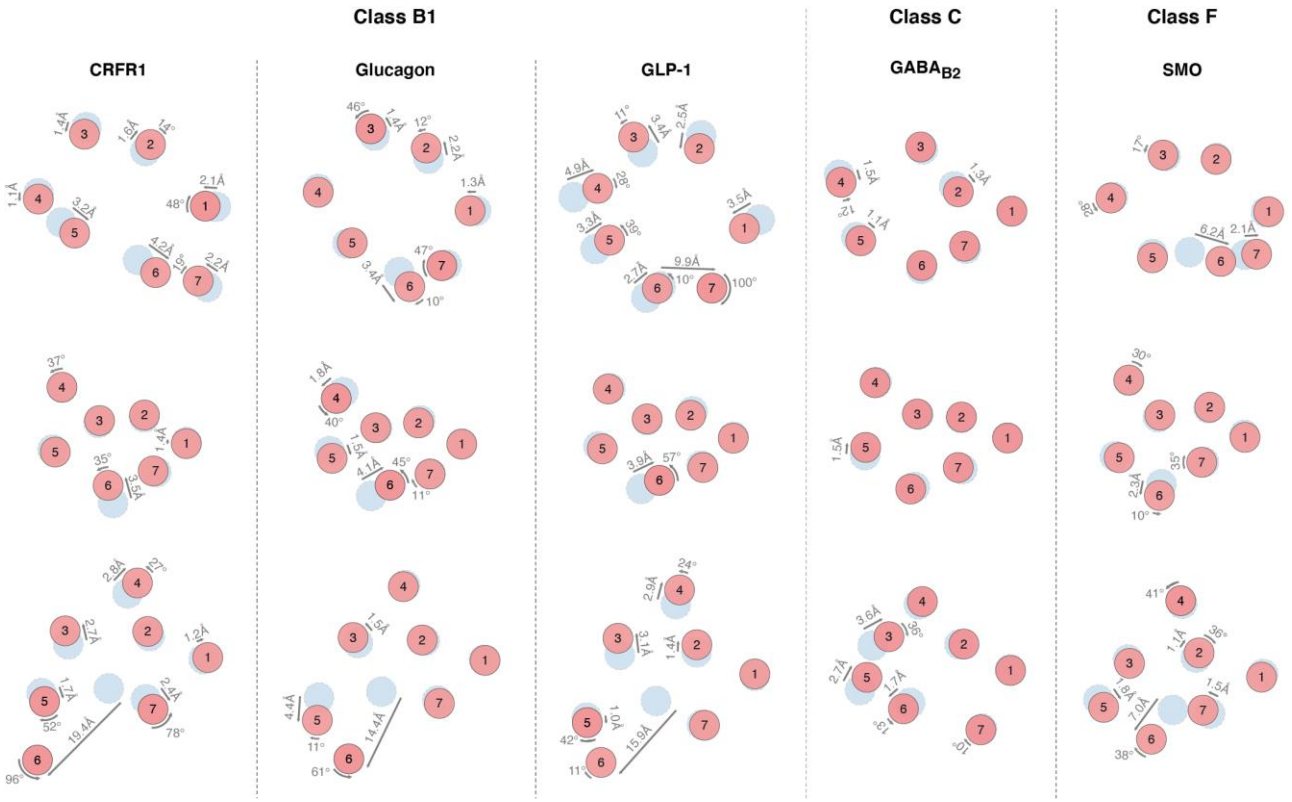

Extended Data Fig. 2 | TM1-7 movement of class B1, C and F receptor pairs upon activation. Transmembrane helix movement at the extracellular face, membrane mid and intracellular face based on comparison of representative inactive and active state structure pairs of class B1, C and F GPCRs (Extended Data Table 1).

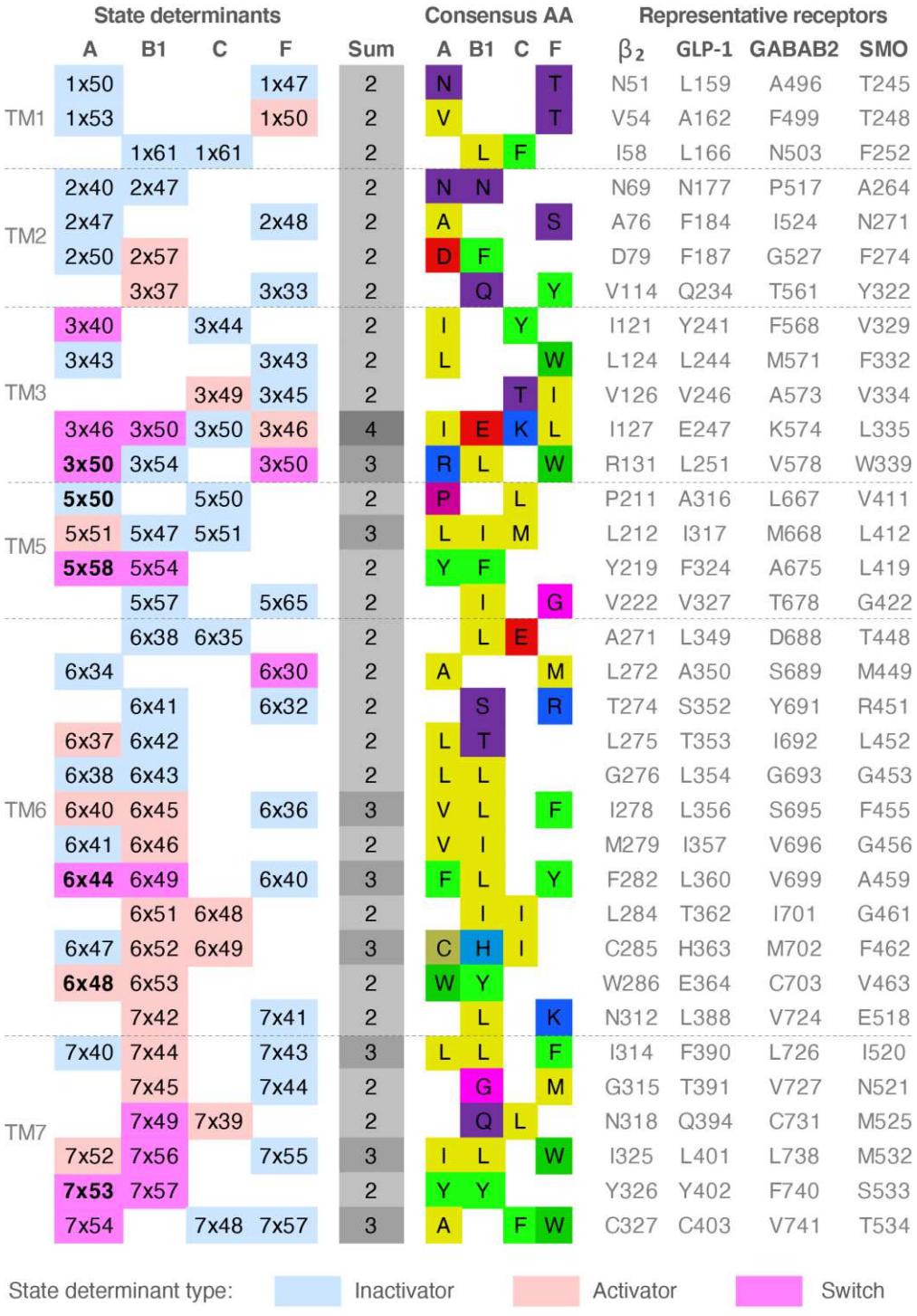

Extended Data Fig. 3 | State determinants conserved across classes. Heatmap of state determinants shared by at least two GPCR classes along with their consensus amino acid and residues in representative receptors. Each row contains corresponding positions denoted with the generic residue numbers in each class[26]. Key class A state determinants are shown in bold.

Extended Data Table 1 | Representative structures of GPCRs and inactive and active states used as templates. The structure annotation and criteria-based filtering to select these templates is shown in Supplementary Spreadsheet 1.

Cl	Receptor family	UniProt	IUPHAR	Inactive PDB ID	Active PDB ID	Inactive Ref.	Active Ref.
A	Adrenoceptors	ADA2B	α_{2B}		6K41		41
A	Cannabinoid	CNR1	CB_1		6N4B		42
A	Chemokine	CCR6	CCR6		6WWZ		43
A	Formylpeptide	FPR2	FPR2/ALX		6OMM		44
A	Neurotensin	NTR1	NTS1		6OS9		45
A	Adrenoceptors	ADRB2	β_2	2RH1	3SN6	36	37
A	Dopamine	DRD3	D_3	3PBL		46	
A	Histamine	HRH1	H_1	3RZE		47	
A	Lysophospholipid (S1P)	S1PR1	$S1P_1$	3V2Y		48	
A	Opioid	OPRK	κ	4DJH		49	
A	Opioid	OPRM	μ	4DKL	6DDE	50	51
A	Opioid	OPRD	δ	4N6H		52	
A	Acetylcholine (muscarinic)	ACM3	M_3	4U15		53	
A	Lysophospholipid (LPA)	LPAR1	LPA_1	4Z36		54	
A	Angiotensin	AGTR1	AT_1	4ZUD		55	
A	Acetylcholine (muscarinic)	ACM1	M_1	5CXV	6OIJ	56	57
A	Opioid	OPRX	NOP	5DHH		58	
A	Acetylcholine (muscarinic)	ACM4	M_4	5DSG		56	
A	Adenosine	AA2AR	A_{2A}	5NM4	5G53	59	60
A	Adenosine	AA1R	A_1	5UEN	6D9H	61	62
A	Dopamine	DRD4	D_4	5WIU		63	
A	Orexin	OX2R	OX_2	5WQC		64	
A	Endothelin	EDNRB	ETB	5X93		65	
A	Neuropeptide Y	NPY1R	Y_1	5ZBQ		66	
A	Acetylcholine (muscarinic)	ACM2	M_2	5ZKC	6OIK	67	57
A	Cannabinoid	CNR2	CB_2	5ZTY	6KPF	68	69
A	5-Hydroxytryptamine	5HT2A	$5\text{-}HT_{2A}$	6A94		70	
A	5-Hydroxytryptamine	5HT2C	$5\text{-}HT_{2C}$	6BQH		71	
A	Complement peptide	C5AR1	$C5a_1$	6C1R		72	
A	Dopamine	DRD2	D_2	6CM4		73	
A	Tachykinin	NK1R	NK_1	6HLP		74	
A	Ghrelin	GHSR	Ghrelin	6KO5		75	
A	Adrenoceptors	ADA2C	α_{2C}	6KUW		76	
A	Chemokine	CXCR2	CXCR2	6LFL	6LFO	77	77
A	Acetylcholine (muscarinic)	ACM5	M_5	6OL9		78	
A	Melatonin	MTR1A	MT_1	6PS8		79	
A	Orexin	OX1R	OX_1	6TOD		80	
A	Vasopressin and oxytocin	OXYR	OT	6TPK		81	
B1	Calcitonin	CALCR	CT		6NIY		82
B1	Calcitonin	CALRL	Calcitonin-like		6UVA		83
B1	Corticotropin-releasing factor	CRFR2	CRF2		6PB1		84
B1	Glucagon	SCTR	Secretin		6WZG		85
B1	VIP and PACAP	PACR	PAC1		6M1I		86
B1	VIP and PACAP	VIPR1	VPAC1		6VN7		87
B1	Corticotropin-releasing factor	CRFR1	CRF1	4K5Y	6P9X	84	20
B1	Glucagon	GLR	Glucagon	5EE7	6WPW	88	21
B1	Parathyroid hormone	PTH1R	PTH1		6NBH		89
B1	Glucagon	GLP1R	GLP-1	6LN2	6X18	18	22
C	Metabotropic glutamate	GRM1	$mGlu_1$	4OR2		90	
C	Metabotropic glutamate	GRM5	$mGlu_5$	6FFI		91	
C	GABAB	GABR1	$GABA_{B1}$	7C7S		38	
C	GABAB	GABR2	$GABA_{B2}$	7C7S	7C7Q	38	38
F	Frizzled	SMO	SMO	4JKV	6XBK	39	40
F	Frizzled	FZD4	FZD_4	6BD4		92	
F	Frizzled	FZD5	FZD_5	6WW2		93	

Supplemental Excel spreadsheets

Supplementary Spreadsheet 1. GPCR structure annotation to define activation states and representative templates

Excel file containing an annotation of all 488 GPCR structures released in the Protein Data Bank[94] before November 1st 2020. Representative structures of each GPCR and inactive or active state were selected by applying comprehensive filter criteria spanning completeness of receptor and G protein (≥86% and ≥43% of generic residue positions, respectively), sequence identity >90% to human, resolution ≤4.0 Å, degree active (≤20% and ≥90% for inactive and active structures, respectively) and consistent ligand modality and state (inverse agonist/antagonist-inactive and agonist-active). A continuous annotation is provided in the GPCRdb structure browser (http://review.gpcrdb.org/structure) and the structure comparison webserver (Extended Data Fig. 1).

Supplementary Spreadsheet 2. Topological and functional mapping of the state determinant positions

Mapping of state determinant 309 ligand and 103 G protein interacting positions (grey and orange fill, respectively) extracted here from 423 GPCR crystal and cryo-EM structures. Each residue position has been assigned one main role defined by ligand and G protein interacting positions located within the intracellular and extracellular TM helix bundle pockets, respectively, and signal transduction pathway residue bridging such positions on the same helix in at least two classes (Methods).

Methods

Structure annotation and selection of representative template dataset. We extended the GPCRdb structures (http://review.gpcrdb.org/structure, all 488 GPCR structures released in the Protein Data Bank[95] before November 1st 2020) with additional annotation. We selected a representative structure of each GPCR and inactive or active state by applying comprehensive filter criteria spanning completeness of receptor and G protein (≥83% and ≥43% of generic residue positions, respectively), sequence identity >90% to human, resolution ≤3.7 Å, degree active[96] (≤20% and ≥90% for inactive and active structures, respectively) and consistent ligand modality and state[96] (inverse agonist/antagonist-inactive and agonist-active). For representative templates of the active state, a G protein complex was required. (Supplementary Spreadsheet 1)

Transmembrane helix rearrangement analysis. 2D plots for TM1-7 segment movement at the extracellular end, cytosolic end and membrane mid, respectively, were produced using our new webserver for comparative structure analysis (http://review.gpcrdb.org/structure_comparison/comparative_analysis and [96]). Class counts of moving TM1-7 were calculated as the sum of consensus movements above 1.0 Å (for class C, priority is given to the Gi-$GABA_{B2}$ over the non-coupled mGluR5 structure).

Segment (TM1-7, H8 and loops) contact analysis. Activation-dependent changes in segment networks were determined using 2D network plots of segment contacts[96]. Segments switches (or helix switches) were defined as the segments with distinct contacts (see next section) in both states.

Generic residue numbering. Corresponding residue positions in each class were indexed with the structure-based GPCRdb generic residue numbering system[26]. This builds on the sequence-based generic residue numbering systems for class A (Ballesteros-Weinstein), B1 (Wootten), C (Pin) and F (Wang), but preserves gaps from a structural alignment of two receptors, caused by a unique helix bulge or constriction, in the sequence alignment thereby avoiding offset of such and following residues. All schemes assign residue numbers relative to the most conserved amino acid residue, which is given the number 50, and prefixed with

the TM helix number (e.g. 3x32 is on TM3 and 18 positions before the reference). This generic residue numbering scheme also uniquely indexes helix 8 and structurally conserved loop segments, which are numbered by the preceding and following TM helix (e.g. 45 is ECL2 located between TM4-5).

State stabilising contact identification. State stabilising contacts were identified using the Structure comparison tool[96]. The most distinct contact in class A (1x49-7x50 contact) has 80% higher frequency in the inactive than active state, and the specificity of state-specific contacts depends on the number of members and templates in each class. To obtain comparable number of networks and contacts, we therefore adjusted the class frequency difference thresholds accordingly (no. members and inactive/active state templates); A: 40% (285, 33/14), B1: 67% (15, 3/10), C: 75% (22, 4/1) and F: 100% (11, 3/1). To ensure that the identified determinants are have a wide role in each class, we applied a sequence conservation cut-off. This cut-off requires the amino acids pairs that make up a state specific contact to be conserved, and therefore be able to form, in at least 30% of all receptors in the given GPCR class. The remaining residues, referred to as "state determinants" or "state stabilisers" were further classified into 'inactivators', 'activators' and 'switches' based on if their most frequent contact occurs in inactive, active and both states, respectively.

State determinant topological mapping in relation to ligand and G protein sites. We mapped state stabilisers to functional sites to ligand and G protein sites using GPCRdb's comparative structure analysis tool[96]. For positions with both an allosteric ligand and G protein interaction, precedence is given to the latter in the snakeplot data mapping (but both are counted in Fig. 5). Determinants located in positions with no known ligand or G protein interactions were categorised as "Other" in our analysis.

Data availability

All data are available in GPCRdb (https://review.gpcrdb.org), GitHub (https://github.com/protwis/gpcrdb_data) and Supplementary Spreadsheets 1-2.

Code availability

No code was developed for this manuscript which instead used the existing GPCRdb[97] resources, including a new comparative structure analysis platform[96]. All open-source code can be obtained from GitHub (https://github.com/protwis/protwis) under the permissive Apache 2.0 License (https://www.apache.org/licenses/LICENSE-2.0). A complete list of the software used for data analysis is available from the Nature Research Reporting Summary.

References

18 Wu, F. *et al.* Full-length human GLP-1 receptor structure without orthosteric ligands. *Nat Commun* **11**, 1272, doi:10.1038/s41467-020-14934-5 (2020).

20 Liang, Y. L. *et al.* Toward a Structural Understanding of Class B GPCR Peptide Binding and Activation. *Mol. Cell* **77**, 656-668 e655, doi:10.1016/j.molcel.2020.01.012 (2020).

21 Hilger, D. *et al.* Structural insights into differences in G protein activation by family A and family B GPCRs. *Science* **369**, eaba3373, doi:10.1126/science.aba3373 (2020).

22 Zhang, X. *et al.* Differential GLP-1R Binding and Activation by Peptide and Non-peptide Agonists. *Mol. Cell* **80**, 485-500 e487, doi:10.1016/j.molcel.2020.09.020 (2020).

26 Isberg, V. *et al.* Generic GPCR residue numbers - aligning topology maps while minding the gaps. *Trends in pharmacological sciences* **36**, 22-31, doi:10.1016/j.tips.2014.11.001 (2015).

36 Cherezov, V. *et al.* High-resolution crystal structure of an engineered human beta2-adrenergic G protein-coupled receptor. *Science* **318**, 1258-1265, doi:10.1126/science.1150577 (2007).

37 Rasmussen, S. G. *et al.* Crystal structure of the beta2 adrenergic receptor-Gs protein complex. *Nature* **477**, 549-555, doi:10.1038/nature10361 (2011).

38 Mao, C. *et al.* Cryo-EM structures of inactive and active GABAB receptor. *Cell Res.* **30**, 564-573, doi:10.1038/s41422-020-0350-5 (2020).

39 Wang, C. *et al.* Structure of the human smoothened receptor bound to an antitumour agent. *Nature* **497**, 338-343, doi:10.1038/nature12167 (2013).

40 Qi, X., Friedberg, L., De Bose-Boyd, R., Long, T. & Li, X. Sterols in an intramolecular channel of Smoothened mediate Hedgehog signaling. *Nat. Chem. Biol.* **16**, 1368-1375, doi:10.1038/s41589-020-0646-2 (2020).

41 Yuan, D. *et al.* Activation of the alpha2B adrenoceptor by the sedative sympatholytic dexmedetomidine. *Nat. Chem. Biol.* **16**, 507-512, doi:10.1038/s41589-020-0492-2 (2020).

42 Krishna Kumar, K. *et al.* Structure of a Signaling Cannabinoid Receptor 1-G Protein Complex. *Cell* **176**, 448-458 e412, doi:10.1016/j.cell.2018.11.040 (2019).

43 Wasilko, D. J. *et al.* Structural basis for chemokine receptor CCR6 activation by the endogenous protein ligand CCL20. *Nat Commun* **11**, 3031, doi:10.1038/s41467-020-16820-6 (2020).

44 Zhuang, Y. *et al.* Structure of formylpeptide receptor 2-Gi complex reveals insights into ligand recognition and signaling. *Nat Commun* **11**, 885, doi:10.1038/s41467-020-14728-9 (2020).

45 Kato, H. E. *et al.* Conformational transitions of a neurotensin receptor 1-Gi1 complex. *Nature* **572**, 80-85, doi:10.1038/s41586-019-1337-6 (2019).

46 Chien, E. Y. *et al.* Structure of the human dopamine D3 receptor in complex with a D2/D3 selective antagonist. *Science* **330**, 1091-1095, doi:10.1126/science.1197410 (2010).

47 Shimamura, T. *et al.* Structure of the human histamine H1 receptor complex with doxepin. *Nature* **475**, 65-70, doi:10.1038/nature10236 (2011).

48 Hanson, M. A. *et al.* Crystal structure of a lipid G protein-coupled receptor. *Science* **335**, 851-855, doi:10.1126/science.1215904 (2012).

49 Wu, H. *et al.* Structure of the human kappa-opioid receptor in complex with JDTic. *Nature* **485**, 327-332, doi:10.1038/nature10939 (2012).

50 Manglik, A. *et al.* Crystal structure of the micro-opioid receptor bound to a morphinan antagonist. *Nature* **485**, 321-326, doi:10.1038/nature10954 (2012).

51 Koehl, A. *et al.* Structure of the micro-opioid receptor-Gi protein complex. *Nature* **558**, 547-552, doi:10.1038/s41586-018-0219-7 (2018).

52 Fenalti, G. *et al.* Molecular control of delta-opioid receptor signalling. *Nature* **506**, 191-196, doi:10.1038/nature12944 (2014).

53 Thorsen, T. S., Matt, R., Weis, W. I. & Kobilka, B. K. Modified T4 Lysozyme Fusion Proteins Facilitate G Protein-Coupled Receptor Crystallogenesis. *Structure* **22**, 1657-1664, doi:10.1016/j.str.2014.08.022 (2014).

54 Chrencik, J. E. *et al.* Crystal Structure of Antagonist Bound Human Lysophosphatidic Acid Receptor 1. *Cell* **161**, 1633-1643, doi:10.1016/j.cell.2015.06.002 (2015).

55 Zhang, H. *et al.* Structural Basis for Ligand Recognition and Functional Selectivity at Angiotensin Receptor. *The Journal of biological chemistry* **290**, 29127-29139, doi:10.1074/jbc.M115.689000 (2015).

56 Thal, D. M. *et al.* Crystal structures of the M1 and M4 muscarinic acetylcholine receptors. *Nature* **531**, 335-340, doi:10.1038/nature17188 (2016).

57 Maeda, S., Qu, Q., Robertson, M. J., Skiniotis, G. & Kobilka, B. K. Structures of the M1 and M2 muscarinic acetylcholine receptor/G-protein complexes. *Science* **364**, 552-557, doi:10.1126/science.aaw5188 (2019).

58 Miller, R. L. *et al.* The Importance of Ligand-Receptor Conformational Pairs in Stabilization: Spotlight on the N/OFQ G Protein-Coupled Receptor. *Structure* **23**, 2291-2299, doi:10.1016/j.str.2015.07.024 (2015).

59 Weinert, T. *et al.* Serial millisecond crystallography for routine room-temperature structure determination at synchrotrons. *Nat Commun* **8**, 542, doi:10.1038/s41467-017-00630-4 (2017).

60 Carpenter, B., Nehme, R., Warne, T., Leslie, A. G. & Tate, C. G. Structure of the adenosine A(2A) receptor bound to an engineered G protein. *Nature* **536**, 104-107, doi:10.1038/nature18966 (2016).

61 Glukhova, A. *et al.* Structure of the Adenosine A1 Receptor Reveals the Basis for Subtype Selectivity. *Cell* **168**, 867-877 e813, doi:10.1016/j.cell.2017.01.042 (2017).

62 Draper-Joyce, C. J. *et al.* Structure of the adenosine-bound human adenosine A1 receptor-Gi complex. *Nature* **558**, 559-563, doi:10.1038/s41586-018-0236-6 (2018).

63 Wang, S. *et al.* D4 dopamine receptor high-resolution structures enable the discovery of selective agonists. *Science* **358**, 381-386, doi:10.1126/science.aan5468 (2017).

64 Suno, R. *et al.* Crystal Structures of Human Orexin 2 Receptor Bound to the Subtype-Selective Antagonist EMPA. *Structure* **26**, 7-19 e15, doi:10.1016/j.str.2017.11.005 (2018).

65 Shihoya, W. *et al.* X-ray structures of endothelin ETB receptor bound to clinical antagonist bosentan and its analog. *Nat. Struct. Mol. Biol.* **24**, 758-764, doi:10.1038/nsmb.3450 (2017).

66 Yang, Z. *et al.* Structural basis of ligand binding modes at the neuropeptide Y Y1 receptor. *Nature* **556**, 520-524, doi:10.1038/s41586-018-0046-x (2018).

67 Suno, R. *et al.* Structural insights into the subtype-selective antagonist binding to the M2 muscarinic receptor. *Nat. Chem. Biol.* **14**, 1150-1158, doi:10.1038/s41589-018-0152-y (2018).

68 Li, X. *et al.* Crystal Structure of the Human Cannabinoid Receptor CB2. *Cell* **176**, 459-467 e413, doi:10.1016/j.cell.2018.12.011 (2019).

69 Hua, T. *et al.* Activation and Signaling Mechanism Revealed by Cannabinoid Receptor-Gi Complex Structures. *Cell* **180**, 655-665 e618, doi:10.1016/j.cell.2020.01.008 (2020).

70 Kimura, K. T. *et al.* Structures of the 5-HT2A receptor in complex with the antipsychotics risperidone and zotepine. *Nat. Struct. Mol. Biol.* **26**, 121-128, doi:10.1038/s41594-018-0180-z (2019).

71 Peng, Y. *et al.* 5-HT2C Receptor Structures Reveal the Structural Basis of GPCR Polypharmacology. *Cell* **172**, 719-730 e714, doi:10.1016/j.cell.2018.01.001 (2018).

72 Liu, H. *et al.* Orthosteric and allosteric action of the C5a receptor antagonists. *Nat. Struct. Mol. Biol.* **25**, 472-481, doi:10.1038/s41594-018-0067-z (2018).

73 Wang, S. *et al.* Structure of the D2 dopamine receptor bound to the atypical antipsychotic drug risperidone. *Nature* **555**, 269-273, doi:10.1038/nature25758 (2018).

74 Schoppe, J. *et al.* Crystal structures of the human neurokinin 1 receptor in complex with clinically used antagonists. *Nat Commun* **10**, 17, doi:10.1038/s41467-018-07939-8 (2019).

75 Shiimura, Y. *et al.* Structure of an antagonist-bound ghrelin receptor reveals possible ghrelin recognition mode. *Nat Commun* **11**, 4160, doi:10.1038/s41467-020-17554-1 (2020).

76 Chen, X. *et al.* Molecular Mechanism for Ligand Recognition and Subtype Selectivity of alpha2C Adrenergic Receptor. *Cell reports* **29**, 2936-2943 e2934, doi:10.1016/j.celrep.2019.10.112 (2019).

77 Liu, K. *et al.* Structural basis of CXC chemokine receptor 2 activation and signalling. *Nature* **585**, 135-140, doi:10.1038/s41586-020-2492-5 (2020).

78 Vuckovic, Z. *et al.* Crystal structure of the M5 muscarinic acetylcholine receptor. *Proceedings of the National Academy of Sciences of the United States of America* **116**, 26001-26007, doi:10.1073/pnas.1914446116 (2019).

79 Ishchenko, A. *et al.* Toward G protein-coupled receptor structure-based drug design using X-ray lasers. *IUCrJ* **6**, 1106-1119, doi:10.1107/S2052252519013137 (2019).

80 Rappas, M. *et al.* Comparison of Orexin 1 and Orexin 2 Ligand Binding Modes Using X-ray Crystallography and Computational Analysis. *Journal of medicinal chemistry* **63**, 1528-1543, doi:10.1021/acs.jmedchem.9b01787 (2020).

81 Waltenspuhl, Y., Schoppe, J., Ehrenmann, J., Kummer, L. & Pluckthun, A. Crystal structure of the human oxytocin receptor. *Sci Adv* **6**, eabb5419, doi:10.1126/sciadv.abb5419 (2020).

82 Dal Maso, E. *et al.* The Molecular Control of Calcitonin Receptor Signaling. *ACS Pharmacol Transl Sci* **2**, 31-51, doi:10.1021/acsptsci.8b00056 (2019).

83 Liang, Y. L. *et al.* Structure and Dynamics of Adrenomedullin Receptors AM1 and AM2 Reveal Key Mechanisms in the Control of Receptor Phenotype by Receptor Activity-Modifying Proteins. *ACS Pharmacol Transl Sci* **3**, 263-284, doi:10.1021/acsptsci.9b00080 (2020).

84 Hollenstein, K. *et al.* Structure of class B GPCR corticotropin-releasing factor receptor 1. *Nature* **499**, 438-443, doi:10.1038/nature12357 (2013).

85 Dong, M. *et al.* Structure and dynamics of the active Gs-coupled human secretin receptor. *Nat Commun* **11**, 4137, doi:10.1038/s41467-020-17791-4 (2020).

86 Wang, J. *et al.* Cryo-EM structures of PAC1 receptor reveal ligand binding mechanism. *Cell Res.* **30**, 436-445, doi:10.1038/s41422-020-0280-2 (2020).

87 Duan, J. *et al.* Cryo-EM structure of an activated VIP1 receptor-G protein complex revealed by a NanoBiT tethering strategy. *Nat Commun* **11**, 4121, doi:10.1038/s41467-020-17933-8 (2020).

88 Jazayeri, A. *et al.* Extra-helical binding site of a glucagon receptor antagonist. *Nature* **533**, 274-277, doi:10.1038/nature17414 (2016).

89 Zhao, L. H. *et al.* Structure and dynamics of the active human parathyroid hormone receptor-1. *Science* **364**, 148-153, doi:10.1126/science.aav7942 (2019).

90 Wu, H. *et al.* Structure of a class C GPCR metabotropic glutamate receptor 1 bound to an allosteric modulator. *Science* **344**, 58-64, doi:10.1126/science.1249489 (2014).

91 Christopher, J. A. *et al.* Structure-Based Optimization Strategies for G Protein-Coupled Receptor (GPCR) Allosteric Modulators: A Case Study from Analyses of New Metabotropic Glutamate Receptor 5 (mGlu5) X-ray Structures. *Journal of medicinal chemistry* **62**, 207-222, doi:10.1021/acs.jmedchem.7b01722 (2019).

92 Yang, S. *et al.* Crystal structure of the Frizzled 4 receptor in a ligand-free state. *Nature* **560**, 666-670, doi:10.1038/s41586-018-0447-x (2018).

93 Tsutsumi, N. *et al.* Structure of human Frizzled5 by fiducial-assisted cryo-EM supports a heterodimeric mechanism of canonical Wnt signaling. *Elife* **9**, doi:10.7554/eLife.58464 (2020).

94 Burley, S. K. *et al.* RCSB Protein Data Bank: biological macromolecular structures enabling research and education in fundamental biology, biomedicine, biotechnology and energy. *Nucleic Acids Res.* **47**, D464-D474, doi:10.1093/nar/gky1004 (2019).

95 Armstrong, D. R. *et al.* PDBe: improved findability of macromolecular structure data in the PDB. *Nucleic Acids Res.* **48**, D335-D343, doi:10.1093/nar/gkz990 (2020).

96 Kooistra, A. J., Munk, C., Hauser, A. S. & Gloriam, D. E. An online GPCR structure analysis platform. *Submitted*.

97 Kooistra, A. J. *et al.* GPCRdb in 2021: integrating GPCR sequence, structure and function. *Nucleic Acids Res.* **49**, D335-D343, doi:10.1093/nar/gkaa1080 (2021).

18 Wu, F. *et al.* Full-length human GLP-1 receptor structure without orthosteric ligands. *Nat Commun* **11**, 1272, doi:10.1038/s41467-020-14934-5 (2020).

20 Liang, Y. L. *et al.* Toward a Structural Understanding of Class B GPCR Peptide Binding and Activation. *Mol. Cell* **77**, 656-668 e655, doi:10.1016/j.molcel.2020.01.012 (2020).

21 Hilger, D. *et al.* Structural insights into differences in G protein activation by family A and family B GPCRs. *Science* **369**, eaba3373, doi:10.1126/science.aba3373 (2020).

22 Zhang, X. *et al.* Differential GLP-1R Binding and Activation by Peptide and Non-peptide Agonists. *Mol. Cell* **80**, 485-500 e487, doi:10.1016/j.molcel.2020.09.020 (2020).

26 Isberg, V. *et al.* Generic GPCR residue numbers - aligning topology maps while minding the gaps. *Trends in pharmacological sciences* **36**, 22-31, doi:10.1016/j.tips.2014.11.001 (2015).

36 Cherezov, V. *et al.* High-resolution crystal structure of an engineered human beta2-adrenergic G protein-coupled receptor. *Science* **318**, 1258-1265, doi:10.1126/science.1150577 (2007).

37 Rasmussen, S. G. *et al.* Crystal structure of the beta2 adrenergic receptor-Gs protein complex. *Nature* **477**, 549-555, doi:10.1038/nature10361 (2011).

38 Mao, C. *et al.* Cryo-EM structures of inactive and active GABAB receptor. *Cell Res.* **30**, 564-573, doi:10.1038/s41422-020-0350-5 (2020).

39 Wang, C. *et al.* Structure of the human smoothened receptor bound to an antitumour agent. *Nature* **497**, 338-343, doi:10.1038/nature12167 (2013).

40 Qi, X., Friedberg, L., De Bose-Boyd, R., Long, T. & Li, X. Sterols in an intramolecular channel of Smoothened mediate Hedgehog signaling. *Nat. Chem. Biol.* **16**, 1368-1375, doi:10.1038/s41589-020-0646-2 (2020).

41 Yuan, D. *et al.* Activation of the alpha2B adrenoceptor by the sedative sympatholytic dexmedetomidine. *Nat. Chem. Biol.* **16**, 507-512, doi:10.1038/s41589-020-0492-2 (2020).

42 Krishna Kumar, K. *et al.* Structure of a Signaling Cannabinoid Receptor 1-G Protein Complex. *Cell* **176**, 448-458 e412, doi:10.1016/j.cell.2018.11.040 (2019).

43 Wasilko, D. J. *et al.* Structural basis for chemokine receptor CCR6 activation by the endogenous protein ligand CCL20. *Nat Commun* **11**, 3031, doi:10.1038/s41467-020-16820-6 (2020).

44 Zhuang, Y. *et al.* Structure of formylpeptide receptor 2-Gi complex reveals insights into ligand recognition and signaling. *Nat Commun* **11**, 885, doi:10.1038/s41467-020-14728-9 (2020).

45 Kato, H. E. *et al.* Conformational transitions of a neurotensin receptor 1-Gi1 complex. *Nature* **572**, 80-85, doi:10.1038/s41586-019-1337-6 (2019).

46 Chien, E. Y. *et al.* Structure of the human dopamine D3 receptor in complex with a D2/D3 selective antagonist. *Science* **330**, 1091-1095, doi:10.1126/science.1197410 (2010).

47 Shimamura, T. *et al.* Structure of the human histamine H1 receptor complex with doxepin. *Nature* **475**, 65-70, doi:10.1038/nature10236 (2011).

48 Hanson, M. A. *et al.* Crystal structure of a lipid G protein-coupled receptor. *Science* **335**, 851-855, doi:10.1126/science.1215904 (2012).

49 Wu, H. *et al.* Structure of the human kappa-opioid receptor in complex with JDTic. *Nature* **485**, 327-332, doi:10.1038/nature10939 (2012).

50 Manglik, A. *et al.* Crystal structure of the micro-opioid receptor bound to a morphinan antagonist. *Nature* **485**, 321-326, doi:10.1038/nature10954 (2012).

51 Koehl, A. *et al.* Structure of the micro-opioid receptor-Gi protein complex. *Nature* **558**, 547-552, doi:10.1038/s41586-018-0219-7 (2018).

52 Fenalti, G. *et al.* Molecular control of delta-opioid receptor signalling. *Nature* **506**, 191-196, doi:10.1038/nature12944 (2014).

53 Thorsen, T. S., Matt, R., Weis, W. I. & Kobilka, B. K. Modified T4 Lysozyme Fusion Proteins Facilitate G Protein-Coupled Receptor Crystallogenesis. *Structure* **22**, 1657-1664, doi:10.1016/j.str.2014.08.022 (2014).

54 Chrencik, J. E. *et al.* Crystal Structure of Antagonist Bound Human Lysophosphatidic Acid Receptor 1. *Cell* **161**, 1633-1643, doi:10.1016/j.cell.2015.06.002 (2015).

55 Zhang, H. *et al.* Structural Basis for Ligand Recognition and Functional Selectivity at Angiotensin Receptor. *The Journal of biological chemistry* **290**, 29127-29139, doi:10.1074/jbc.M115.689000 (2015).

56 Thal, D. M. *et al.* Crystal structures of the M1 and M4 muscarinic acetylcholine receptors. *Nature* **531**, 335-340, doi:10.1038/nature17188 (2016).

57 Maeda, S., Qu, Q., Robertson, M. J., Skiniotis, G. & Kobilka, B. K. Structures of the M1 and M2 muscarinic acetylcholine receptor/G-protein complexes. *Science* **364**, 552-557, doi:10.1126/science.aaw5188 (2019).

58 Miller, R. L. *et al.* The Importance of Ligand-Receptor Conformational Pairs in Stabilization: Spotlight on the N/OFQ G Protein-Coupled Receptor. *Structure* **23**, 2291-2299, doi:10.1016/j.str.2015.07.024 (2015).

59 Weinert, T. *et al.* Serial millisecond crystallography for routine room-temperature structure determination at synchrotrons. *Nat Commun* **8**, 542, doi:10.1038/s41467-017-00630-4 (2017).

60 Carpenter, B., Nehme, R., Warne, T., Leslie, A. G. & Tate, C. G. Structure of the adenosine A(2A) receptor bound to an engineered G protein. *Nature* **536**, 104-107, doi:10.1038/nature18966 (2016).

61 Glukhova, A. *et al.* Structure of the Adenosine A1 Receptor Reveals the Basis for Subtype Selectivity. *Cell* **168**, 867-877 e813, doi:10.1016/j.cell.2017.01.042 (2017).

62 Draper-Joyce, C. J. *et al.* Structure of the adenosine-bound human adenosine A1 receptor-Gi complex. *Nature* **558**, 559-563, doi:10.1038/s41586-018-0236-6 (2018).

63 Wang, S. *et al.* D4 dopamine receptor high-resolution structures enable the discovery of selective agonists. *Science* **358**, 381-386, doi:10.1126/science.aan5468 (2017).

64 Suno, R. *et al.* Crystal Structures of Human Orexin 2 Receptor Bound to the Subtype-Selective Antagonist EMPA. *Structure* **26**, 7-19 e15, doi:10.1016/j.str.2017.11.005 (2018).

65 Shihoya, W. *et al.* X-ray structures of endothelin ETB receptor bound to clinical antagonist bosentan and its analog. *Nat. Struct. Mol. Biol.* **24**, 758-764, doi:10.1038/nsmb.3450 (2017).

66 Yang, Z. *et al.* Structural basis of ligand binding modes at the neuropeptide Y Y1 receptor. *Nature* **556**, 520-524, doi:10.1038/s41586-018-0046-x (2018).

67 Suno, R. *et al.* Structural insights into the subtype-selective antagonist binding to the M2 muscarinic receptor. *Nat. Chem. Biol.* **14**, 1150-1158, doi:10.1038/s41589-018-0152-y (2018).

68 Li, X. *et al.* Crystal Structure of the Human Cannabinoid Receptor CB2. *Cell* **176**, 459-467 e413, doi:10.1016/j.cell.2018.12.011 (2019).

69 Hua, T. *et al.* Activation and Signaling Mechanism Revealed by Cannabinoid Receptor-Gi Complex Structures. *Cell* **180**, 655-665 e618, doi:10.1016/j.cell.2020.01.008 (2020).

70 Kimura, K. T. *et al.* Structures of the 5-HT2A receptor in complex with the antipsychotics risperidone and zotepine. *Nat. Struct. Mol. Biol.* **26**, 121-128, doi:10.1038/s41594-018-0180-z (2019).

71 Peng, Y. *et al.* 5-HT2C Receptor Structures Reveal the Structural Basis of GPCR Polypharmacology. *Cell* **172**, 719-730 e714, doi:10.1016/j.cell.2018.01.001 (2018).

72 Liu, H. *et al.* Orthosteric and allosteric action of the C5a receptor antagonists. *Nat. Struct. Mol. Biol.* **25**, 472-481, doi:10.1038/s41594-018-0067-z (2018).

73 Wang, S. *et al.* Structure of the D2 dopamine receptor bound to the atypical antipsychotic drug risperidone. *Nature* **555**, 269-273, doi:10.1038/nature25758 (2018).

74 Schoppe, J. *et al.* Crystal structures of the human neurokinin 1 receptor in complex with clinically used antagonists. *Nat Commun* **10**, 17, doi:10.1038/s41467-018-07939-8 (2019).

75 Shiimura, Y. *et al.* Structure of an antagonist-bound ghrelin receptor reveals possible ghrelin recognition mode. *Nat Commun* **11**, 4160, doi:10.1038/s41467-020-17554-1 (2020).

76 Chen, X. *et al.* Molecular Mechanism for Ligand Recognition and Subtype Selectivity of alpha2C Adrenergic Receptor. *Cell reports* **29**, 2936-2943 e2934, doi:10.1016/j.celrep.2019.10.112 (2019).

77 Liu, K. *et al.* Structural basis of CXC chemokine receptor 2 activation and signalling. *Nature* **585**, 135-140, doi:10.1038/s41586-020-2492-5 (2020).

78 Vuckovic, Z. *et al.* Crystal structure of the M5 muscarinic acetylcholine receptor. *Proceedings of the National Academy of Sciences of the United States of America* **116**, 26001-26007, doi:10.1073/pnas.1914446116 (2019).

79 Ishchenko, A. *et al.* Toward G protein-coupled receptor structure-based drug design using X-ray lasers. *IUCrJ* **6**, 1106-1119, doi:10.1107/S2052252519013137 (2019).

80 Rappas, M. *et al.* Comparison of Orexin 1 and Orexin 2 Ligand Binding Modes Using X-ray Crystallography and Computational Analysis. *Journal of medicinal chemistry* **63**, 1528-1543, doi:10.1021/acs.jmedchem.9b01787 (2020).

81 Waltenspuhl, Y., Schoppe, J., Ehrenmann, J., Kummer, L. & Pluckthun, A. Crystal structure of the human oxytocin receptor. *Sci Adv* **6**, eabb5419, doi:10.1126/sciadv.abb5419 (2020).

82 Dal Maso, E. *et al.* The Molecular Control of Calcitonin Receptor Signaling. *ACS Pharmacol Transl Sci* **2**, 31-51, doi:10.1021/acsptsci.8b00056 (2019).

83 Liang, Y. L. *et al.* Structure and Dynamics of Adrenomedullin Receptors AM1 and AM2 Reveal Key Mechanisms in the Control of Receptor Phenotype by Receptor Activity-Modifying Proteins. *ACS Pharmacol Transl Sci* **3**, 263-284, doi:10.1021/acsptsci.9b00080 (2020).

84 Hollenstein, K. *et al.* Structure of class B GPCR corticotropin-releasing factor receptor 1. *Nature* **499**, 438-443, doi:10.1038/nature12357 (2013).

85 Dong, M. *et al.* Structure and dynamics of the active Gs-coupled human secretin receptor. *Nat Commun* **11**, 4137, doi:10.1038/s41467-020-17791-4 (2020).

86 Wang, J. *et al.* Cryo-EM structures of PAC1 receptor reveal ligand binding mechanism. *Cell Res.* **30**, 436-445, doi:10.1038/s41422-020-0280-2 (2020).

87 Duan, J. *et al.* Cryo-EM structure of an activated VIP1 receptor-G protein complex revealed by a NanoBiT tethering strategy. *Nat Commun* **11**, 4121, doi:10.1038/s41467-020-17933-8 (2020).

88 Jazayeri, A. *et al.* Extra-helical binding site of a glucagon receptor antagonist. *Nature* **533**, 274-277, doi:10.1038/nature17414 (2016).

89 Zhao, L. H. *et al.* Structure and dynamics of the active human parathyroid hormone receptor-1. *Science* **364**, 148-153, doi:10.1126/science.aav7942 (2019).

90 Wu, H. *et al.* Structure of a class C GPCR metabotropic glutamate receptor 1 bound to an allosteric modulator. *Science* **344**, 58-64, doi:10.1126/science.1249489 (2014).

91 Christopher, J. A. *et al.* Structure-Based Optimization Strategies for G Protein-Coupled Receptor (GPCR) Allosteric Modulators: A Case Study from Analyses of New Metabotropic Glutamate Receptor 5 (mGlu5) X-ray Structures. *Journal of medicinal chemistry* **62**, 207-222, doi:10.1021/acs.jmedchem.7b01722 (2019).

92 Yang, S. *et al.* Crystal structure of the Frizzled 4 receptor in a ligand-free state. *Nature* **560**, 666-670, doi:10.1038/s41586-018-0447-x (2018).

93 Tsutsumi, N. *et al.* Structure of human Frizzled5 by fiducial-assisted cryo-EM supports a heterodimeric mechanism of canonical Wnt signaling. *Elife* **9**, doi:10.7554/eLife.58464 (2020).

94 Burley, S. K. *et al.* RCSB Protein Data Bank: biological macromolecular structures enabling research and education in fundamental biology, biomedicine, biotechnology and energy. *Nucleic Acids Res.* **47**, D464-D474, doi:10.1093/nar/gky1004 (2019).

95 Armstrong, D. R. *et al.* PDBe: improved findability of macromolecular structure data in the PDB. *Nucleic Acids Res.* **48**, D335-D343, doi:10.1093/nar/gkz990 (2020).

96 Kooistra, A. J., Munk, C., Hauser, A. S. & Gloriam, D. E. An online platform for comparative GPCR structure analysis. *Submitted*.

97 Kooistra, A. J. *et al.* GPCRdb in 2021: integrating GPCR sequence, structure and function. *Nucleic Acids Res.* **49**, D335-D343, doi:10.1093/nar/gkaa1080 (2021).

18 Wu, F. *et al.* Full-length human GLP-1 receptor structure without orthosteric ligands. *Nat Commun* **11**, 1272, doi:10.1038/s41467-020-14934-5 (2020).

20 Liang, Y. L. *et al.* Toward a Structural Understanding of Class B GPCR Peptide Binding and Activation. *Mol. Cell* **77**, 656-668 e655, doi:10.1016/j.molcel.2020.01.012 (2020).

21 Hilger, D. *et al.* Structural insights into differences in G protein activation by family A and family B GPCRs. *Science* **369**, eaba3373, doi:10.1126/science.aba3373 (2020).

22 Zhang, X. *et al.* Differential GLP-1R Binding and Activation by Peptide and Non-peptide Agonists. *Mol. Cell* **80**, 485-500 e487, doi:10.1016/j.molcel.2020.09.020 (2020).

26 Isberg, V. *et al.* Generic GPCR residue numbers - aligning topology maps while minding the gaps. *Trends in pharmacological sciences* **36**, 22-31, doi:10.1016/j.tips.2014.11.001 (2015).

36 Cherezov, V. *et al.* High-resolution crystal structure of an engineered human beta2-adrenergic G protein-coupled receptor. *Science* **318**, 1258-1265, doi:10.1126/science.1150577 (2007).

37 Rasmussen, S. G. *et al.* Crystal structure of the beta2 adrenergic receptor-Gs protein complex. *Nature* **477**, 549-555, doi:10.1038/nature10361 (2011).

38 Mao, C. *et al.* Cryo-EM structures of inactive and active GABAB receptor. *Cell Res.* **30**, 564-573, doi:10.1038/s41422-020-0350-5 (2020).

39 Wang, C. *et al.* Structure of the human smoothened receptor bound to an antitumour agent. *Nature* **497**, 338-343, doi:10.1038/nature12167 (2013).

40 Qi, X., Friedberg, L., De Bose-Boyd, R., Long, T. & Li, X. Sterols in an intramolecular channel of Smoothened mediate Hedgehog signaling. *Nat. Chem. Biol.* **16**, 1368-1375, doi:10.1038/s41589-020-0646-2 (2020).

41 Yuan, D. *et al.* Activation of the alpha2B adrenoceptor by the sedative sympatholytic dexmedetomidine. *Nat. Chem. Biol.* **16**, 507-512, doi:10.1038/s41589-020-0492-2 (2020).

42 Krishna Kumar, K. *et al.* Structure of a Signaling Cannabinoid Receptor 1-G Protein Complex. *Cell* **176**, 448-458 e412, doi:10.1016/j.cell.2018.11.040 (2019).

43 Wasilko, D. J. *et al.* Structural basis for chemokine receptor CCR6 activation by the endogenous protein ligand CCL20. *Nat Commun* **11**, 3031, doi:10.1038/s41467-020-16820-6 (2020).

44 Zhuang, Y. *et al.* Structure of formylpeptide receptor 2-Gi complex reveals insights into ligand recognition and signaling. *Nat Commun* **11**, 885, doi:10.1038/s41467-020-14728-9 (2020).

45 Kato, H. E. *et al.* Conformational transitions of a neurotensin receptor 1-Gi1 complex. *Nature* **572**, 80-85, doi:10.1038/s41586-019-1337-6 (2019).

46 Chien, E. Y. *et al.* Structure of the human dopamine D3 receptor in complex with a D2/D3 selective antagonist. *Science* **330**, 1091-1095, doi:10.1126/science.1197410 (2010).

47 Shimamura, T. *et al.* Structure of the human histamine H1 receptor complex with doxepin. *Nature* **475**, 65-70, doi:10.1038/nature10236 (2011).

48 Hanson, M. A. *et al.* Crystal structure of a lipid G protein-coupled receptor. *Science* **335**, 851-855, doi:10.1126/science.1215904 (2012).

49 Wu, H. *et al.* Structure of the human kappa-opioid receptor in complex with JDTic. *Nature* **485**, 327-332, doi:10.1038/nature10939 (2012).

50 Manglik, A. *et al.* Crystal structure of the micro-opioid receptor bound to a morphinan antagonist. *Nature* **485**, 321-326, doi:10.1038/nature10954 (2012).

51 Koehl, A. *et al.* Structure of the micro-opioid receptor-Gi protein complex. *Nature* **558**, 547-552, doi:10.1038/s41586-018-0219-7 (2018).

52 Fenalti, G. *et al.* Molecular control of delta-opioid receptor signalling. *Nature* **506**, 191-196, doi:10.1038/nature12944 (2014).

53 Thorsen, T. S., Matt, R., Weis, W. I. & Kobilka, B. K. Modified T4 Lysozyme Fusion Proteins Facilitate G Protein-Coupled Receptor Crystallogenesis. *Structure* **22**, 1657-1664, doi:10.1016/j.str.2014.08.022 (2014).

54 Chrencik, J. E. *et al.* Crystal Structure of Antagonist Bound Human Lysophosphatidic Acid Receptor 1. *Cell* **161**, 1633-1643, doi:10.1016/j.cell.2015.06.002 (2015).

55 Zhang, H. *et al.* Structural Basis for Ligand Recognition and Functional Selectivity at Angiotensin Receptor. *The Journal of biological chemistry* **290**, 29127-29139, doi:10.1074/jbc.M115.689000 (2015).

56 Thal, D. M. *et al.* Crystal structures of the M1 and M4 muscarinic acetylcholine receptors. *Nature* **531**, 335-340, doi:10.1038/nature17188 (2016).

57 Maeda, S., Qu, Q., Robertson, M. J., Skiniotis, G. & Kobilka, B. K. Structures of the M1 and M2 muscarinic acetylcholine receptor/G-protein complexes. *Science* **364**, 552-557, doi:10.1126/science.aaw5188 (2019).

58 Miller, R. L. *et al.* The Importance of Ligand-Receptor Conformational Pairs in Stabilization: Spotlight on the N/OFQ G Protein-Coupled Receptor. *Structure* **23**, 2291-2299, doi:10.1016/j.str.2015.07.024 (2015).

59 Weinert, T. *et al.* Serial millisecond crystallography for routine room-temperature structure determination at synchrotrons. *Nat Commun* **8**, 542, doi:10.1038/s41467-017-00630-4 (2017).

60 Carpenter, B., Nehme, R., Warne, T., Leslie, A. G. & Tate, C. G. Structure of the adenosine A(2A) receptor bound to an engineered G protein. *Nature* **536**, 104-107, doi:10.1038/nature18966 (2016).

61 Glukhova, A. *et al.* Structure of the Adenosine A1 Receptor Reveals the Basis for Subtype Selectivity. *Cell* **168**, 867-877 e813, doi:10.1016/j.cell.2017.01.042 (2017).

62 Draper-Joyce, C. J. *et al.* Structure of the adenosine-bound human adenosine A1 receptor-Gi complex. *Nature* **558**, 559-563, doi:10.1038/s41586-018-0236-6 (2018).

63 Wang, S. *et al.* D4 dopamine receptor high-resolution structures enable the discovery of selective agonists. *Science* **358**, 381-386, doi:10.1126/science.aan5468 (2017).

64 Suno, R. *et al.* Crystal Structures of Human Orexin 2 Receptor Bound to the Subtype-Selective Antagonist EMPA. *Structure* **26**, 7-19 e15, doi:10.1016/j.str.2017.11.005 (2018).

65 Shihoya, W. *et al.* X-ray structures of endothelin ETB receptor bound to clinical antagonist bosentan and its analog. *Nat. Struct. Mol. Biol.* **24**, 758-764, doi:10.1038/nsmb.3450 (2017).

66 Yang, Z. *et al.* Structural basis of ligand binding modes at the neuropeptide Y Y1 receptor. *Nature* **556**, 520-524, doi:10.1038/s41586-018-0046-x (2018).

67 Suno, R. *et al.* Structural insights into the subtype-selective antagonist binding to the M2 muscarinic receptor. *Nat. Chem. Biol.* **14**, 1150-1158, doi:10.1038/s41589-018-0152-y (2018).

68 Li, X. *et al.* Crystal Structure of the Human Cannabinoid Receptor CB2. *Cell* **176**, 459-467 e413, doi:10.1016/j.cell.2018.12.011 (2019).

69 Hua, T. *et al.* Activation and Signaling Mechanism Revealed by Cannabinoid Receptor-Gi Complex Structures. *Cell* **180**, 655-665 e618, doi:10.1016/j.cell.2020.01.008 (2020).

70 Kimura, K. T. *et al.* Structures of the 5-HT2A receptor in complex with the antipsychotics risperidone and zotepine. *Nat. Struct. Mol. Biol.* **26**, 121-128, doi:10.1038/s41594-018-0180-z (2019).

71 Peng, Y. *et al.* 5-HT2C Receptor Structures Reveal the Structural Basis of GPCR Polypharmacology. *Cell* **172**, 719-730 e714, doi:10.1016/j.cell.2018.01.001 (2018).

72 Liu, H. *et al.* Orthosteric and allosteric action of the C5a receptor antagonists. *Nat. Struct. Mol. Biol.* **25**, 472-481, doi:10.1038/s41594-018-0067-z (2018).

73 Wang, S. *et al.* Structure of the D2 dopamine receptor bound to the atypical antipsychotic drug risperidone. *Nature* **555**, 269-273, doi:10.1038/nature25758 (2018).

74 Schoppe, J. *et al.* Crystal structures of the human neurokinin 1 receptor in complex with clinically used antagonists. *Nat Commun* **10**, 17, doi:10.1038/s41467-018-07939-8 (2019).

75 Shiimura, Y. *et al.* Structure of an antagonist-bound ghrelin receptor reveals possible ghrelin recognition mode. *Nat Commun* **11**, 4160, doi:10.1038/s41467-020-17554-1 (2020).

76 Chen, X. *et al.* Molecular Mechanism for Ligand Recognition and Subtype Selectivity of alpha2C Adrenergic Receptor. *Cell reports* **29**, 2936-2943 e2934, doi:10.1016/j.celrep.2019.10.112 (2019).

77 Liu, K. *et al.* Structural basis of CXC chemokine receptor 2 activation and signalling. *Nature* **585**, 135-140, doi:10.1038/s41586-020-2492-5 (2020).

78 Vuckovic, Z. *et al.* Crystal structure of the M5 muscarinic acetylcholine receptor. *Proceedings of the National Academy of Sciences of the United States of America* **116**, 26001-26007, doi:10.1073/pnas.1914446116 (2019).

79 Ishchenko, A. *et al.* Toward G protein-coupled receptor structure-based drug design using X-ray lasers. *IUCrJ* **6**, 1106-1119, doi:10.1107/S2052252519013137 (2019).

80 Rappas, M. *et al.* Comparison of Orexin 1 and Orexin 2 Ligand Binding Modes Using X-ray Crystallography and Computational Analysis. *Journal of medicinal chemistry* **63**, 1528-1543, doi:10.1021/acs.jmedchem.9b01787 (2020).

81 Waltenspuhl, Y., Schoppe, J., Ehrenmann, J., Kummer, L. & Pluckthun, A. Crystal structure of the human oxytocin receptor. *Sci Adv* **6**, eabb5419, doi:10.1126/sciadv.abb5419 (2020).

82 Dal Maso, E. *et al.* The Molecular Control of Calcitonin Receptor Signaling. *ACS Pharmacol Transl Sci* **2**, 31-51, doi:10.1021/acsptsci.8b00056 (2019).

83 Liang, Y. L. *et al.* Structure and Dynamics of Adrenomedullin Receptors AM1 and AM2 Reveal Key Mechanisms in the Control of Receptor Phenotype by Receptor Activity-Modifying Proteins. *ACS Pharmacol Transl Sci* **3**, 263-284, doi:10.1021/acsptsci.9b00080 (2020).

84 Hollenstein, K. *et al.* Structure of class B GPCR corticotropin-releasing factor receptor 1. *Nature* **499**, 438-443, doi:10.1038/nature12357 (2013).

85 Dong, M. *et al.* Structure and dynamics of the active Gs-coupled human secretin receptor. *Nat Commun* **11**, 4137, doi:10.1038/s41467-020-17791-4 (2020).

86 Wang, J. *et al.* Cryo-EM structures of PAC1 receptor reveal ligand binding mechanism. *Cell Res.* **30**, 436-445, doi:10.1038/s41422-020-0280-2 (2020).

87 Duan, J. *et al.* Cryo-EM structure of an activated VIP1 receptor-G protein complex revealed by a NanoBiT tethering strategy. *Nat Commun* **11**, 4121, doi:10.1038/s41467-020-17933-8 (2020).

88 Jazayeri, A. *et al.* Extra-helical binding site of a glucagon receptor antagonist. *Nature* **533**, 274-277, doi:10.1038/nature17414 (2016).

89 Zhao, L. H. *et al.* Structure and dynamics of the active human parathyroid hormone receptor-1. *Science* **364**, 148-153, doi:10.1126/science.aav7942 (2019).

90 Wu, H. *et al.* Structure of a class C GPCR metabotropic glutamate receptor 1 bound to an allosteric modulator. *Science* **344**, 58-64, doi:10.1126/science.1249489 (2014).

91 Christopher, J. A. *et al.* Structure-Based Optimization Strategies for G Protein-Coupled Receptor (GPCR) Allosteric Modulators: A Case Study from Analyses of New Metabotropic Glutamate Receptor 5 (mGlu5) X-ray Structures. *Journal of medicinal chemistry* **62**, 207-222, doi:10.1021/acs.jmedchem.7b01722 (2019).

92 Yang, S. *et al.* Crystal structure of the Frizzled 4 receptor in a ligand-free state. *Nature* **560**, 666-670, doi:10.1038/s41586-018-0447-x (2018).

93 Tsutsumi, N. *et al.* Structure of human Frizzled5 by fiducial-assisted cryo-EM supports a heterodimeric mechanism of canonical Wnt signaling. *Elife* **9**, doi:10.7554/eLife.58464 (2020).

94 Burley, S. K. *et al.* RCSB Protein Data Bank: biological macromolecular structures enabling research and education in fundamental biology, biomedicine, biotechnology and energy. *Nucleic Acids Res.* **47**, D464-D474, doi:10.1093/nar/gky1004 (2019).

95 Armstrong, D. R. *et al.* PDBe: improved findability of macromolecular structure data in the PDB. *Nucleic Acids Res.* **48**, D335-D343, doi:10.1093/nar/gkz990 (2020).

96 Kooistra, A. J., Munk, C., Hauser, A. S. & Gloriam, D. E. An online resource for comparative GPCR structure analysis. *Submitted*.

18 Wu, F. *et al.* Full-length human GLP-1 receptor structure without orthosteric ligands. *Nat Commun* **11**, 1272, doi:10.1038/s41467-020-14934-5 (2020).

20 Liang, Y. L. *et al.* Toward a Structural Understanding of Class B GPCR Peptide Binding and Activation. *Mol. Cell* **77**, 656-668 e655, doi:10.1016/j.molcel.2020.01.012 (2020).

21 Hilger, D. *et al.* Structural insights into differences in G protein activation by family A and family B GPCRs. *Science* **369**, eaba3373, doi:10.1126/science.aba3373 (2020).

22 Zhang, X. *et al.* Differential GLP-1R Binding and Activation by Peptide and Non-peptide Agonists. *Mol. Cell* **80**, 485-500 e487, doi:10.1016/j.molcel.2020.09.020 (2020).

26 Isberg, V. *et al.* Generic GPCR residue numbers - aligning topology maps while minding the gaps. *Trends in pharmacological sciences* **36**, 22-31, doi:10.1016/j.tips.2014.11.001 (2015).

36 Cherezov, V. *et al.* High-resolution crystal structure of an engineered human beta2-adrenergic G protein-coupled receptor. *Science* **318**, 1258-1265, doi:10.1126/science.1150577 (2007).

37 Rasmussen, S. G. *et al.* Crystal structure of the beta2 adrenergic receptor-Gs protein complex. *Nature* **477**, 549-555, doi:10.1038/nature10361 (2011).

38 Mao, C. *et al.* Cryo-EM structures of inactive and active GABAB receptor. *Cell Res.* **30**, 564-573, doi:10.1038/s41422-020-0350-5 (2020).

39 Wang, C. *et al.* Structure of the human smoothened receptor bound to an antitumour agent. *Nature* **497**, 338-343, doi:10.1038/nature12167 (2013).

40 Qi, X., Friedberg, L., De Bose-Boyd, R., Long, T. & Li, X. Sterols in an intramolecular channel of Smoothened mediate Hedgehog signaling. *Nat. Chem. Biol.* **16**, 1368-1375, doi:10.1038/s41589-020-0646-2 (2020).

41 Yuan, D. *et al.* Activation of the alpha2B adrenoceptor by the sedative sympatholytic dexmedetomidine. *Nat. Chem. Biol.* **16**, 507-512, doi:10.1038/s41589-020-0492-2 (2020).

42 Krishna Kumar, K. *et al.* Structure of a Signaling Cannabinoid Receptor 1-G Protein Complex. *Cell* **176**, 448-458 e412, doi:10.1016/j.cell.2018.11.040 (2019).

43 Wasilko, D. J. *et al.* Structural basis for chemokine receptor CCR6 activation by the endogenous protein ligand CCL20. *Nat Commun* **11**, 3031, doi:10.1038/s41467-020-16820-6 (2020).

44 Zhuang, Y. *et al.* Structure of formylpeptide receptor 2-Gi complex reveals insights into ligand recognition and signaling. *Nat Commun* **11**, 885, doi:10.1038/s41467-020-14728-9 (2020).

45 Kato, H. E. *et al.* Conformational transitions of a neurotensin receptor 1-Gi1 complex. *Nature* **572**, 80-85, doi:10.1038/s41586-019-1337-6 (2019).

46 Chien, E. Y. *et al.* Structure of the human dopamine D3 receptor in complex with a D2/D3 selective antagonist. *Science* **330**, 1091-1095, doi:10.1126/science.1197410 (2010).

47 Shimamura, T. *et al.* Structure of the human histamine H1 receptor complex with doxepin. *Nature* **475**, 65-70, doi:10.1038/nature10236 (2011).

48 Hanson, M. A. *et al.* Crystal structure of a lipid G protein-coupled receptor. *Science* **335**, 851-855, doi:10.1126/science.1215904 (2012).

49 Wu, H. *et al.* Structure of the human kappa-opioid receptor in complex with JDTic. *Nature* **485**, 327-332, doi:10.1038/nature10939 (2012).

50 Manglik, A. *et al.* Crystal structure of the micro-opioid receptor bound to a morphinan antagonist. *Nature* **485**, 321-326, doi:10.1038/nature10954 (2012).

51 Koehl, A. *et al.* Structure of the micro-opioid receptor-Gi protein complex. *Nature* **558**, 547-552, doi:10.1038/s41586-018-0219-7 (2018).

52 Fenalti, G. *et al.* Molecular control of delta-opioid receptor signalling. *Nature* **506**, 191-196, doi:10.1038/nature12944 (2014).

53 Thorsen, T. S., Matt, R., Weis, W. I. & Kobilka, B. K. Modified T4 Lysozyme Fusion Proteins Facilitate G Protein-Coupled Receptor Crystallogenesis. *Structure* **22**, 1657-1664, doi:10.1016/j.str.2014.08.022 (2014).

54 Chrencik, J. E. *et al.* Crystal Structure of Antagonist Bound Human Lysophosphatidic Acid Receptor 1. *Cell* **161**, 1633-1643, doi:10.1016/j.cell.2015.06.002 (2015).

55 Zhang, H. *et al.* Structural Basis for Ligand Recognition and Functional Selectivity at Angiotensin Receptor. *The Journal of biological chemistry* **290**, 29127-29139, doi:10.1074/jbc.M115.689000 (2015).

56 Thal, D. M. *et al.* Crystal structures of the M1 and M4 muscarinic acetylcholine receptors. *Nature* **531**, 335-340, doi:10.1038/nature17188 (2016).

57 Maeda, S., Qu, Q., Robertson, M. J., Skiniotis, G. & Kobilka, B. K. Structures of the M1 and M2 muscarinic acetylcholine receptor/G-protein complexes. *Science* **364**, 552-557, doi:10.1126/science.aaw5188 (2019).

58 Miller, R. L. *et al.* The Importance of Ligand-Receptor Conformational Pairs in Stabilization: Spotlight on the N/OFQ G Protein-Coupled Receptor. *Structure* **23**, 2291-2299, doi:10.1016/j.str.2015.07.024 (2015).

59 Weinert, T. *et al.* Serial millisecond crystallography for routine room-temperature structure determination at synchrotrons. *Nat Commun* **8**, 542, doi:10.1038/s41467-017-00630-4 (2017).

60 Carpenter, B., Nehme, R., Warne, T., Leslie, A. G. & Tate, C. G. Structure of the adenosine A(2A) receptor bound to an engineered G protein. *Nature* **536**, 104-107, doi:10.1038/nature18966 (2016).

61 Glukhova, A. *et al.* Structure of the Adenosine A1 Receptor Reveals the Basis for Subtype Selectivity. *Cell* **168**, 867-877 e813, doi:10.1016/j.cell.2017.01.042 (2017).

62 Draper-Joyce, C. J. *et al.* Structure of the adenosine-bound human adenosine A1 receptor-Gi complex. *Nature* **558**, 559-563, doi:10.1038/s41586-018-0236-6 (2018).

63 Wang, S. *et al.* D4 dopamine receptor high-resolution structures enable the discovery of selective agonists. *Science* **358**, 381-386, doi:10.1126/science.aan5468 (2017).

64 Suno, R. *et al.* Crystal Structures of Human Orexin 2 Receptor Bound to the Subtype-Selective Antagonist EMPA. *Structure* **26**, 7-19 e15, doi:10.1016/j.str.2017.11.005 (2018).

65 Shihoya, W. *et al.* X-ray structures of endothelin ETB receptor bound to clinical antagonist bosentan and its analog. *Nat. Struct. Mol. Biol.* **24**, 758-764, doi:10.1038/nsmb.3450 (2017).

66 Yang, Z. *et al.* Structural basis of ligand binding modes at the neuropeptide Y Y1 receptor. *Nature* **556**, 520-524, doi:10.1038/s41586-018-0046-x (2018).

67 Suno, R. *et al.* Structural insights into the subtype-selective antagonist binding to the M2 muscarinic receptor. *Nat. Chem. Biol.* **14**, 1150-1158, doi:10.1038/s41589-018-0152-y (2018).

68 Li, X. *et al.* Crystal Structure of the Human Cannabinoid Receptor CB2. *Cell* **176**, 459-467 e413, doi:10.1016/j.cell.2018.12.011 (2019).

69 Hua, T. *et al.* Activation and Signaling Mechanism Revealed by Cannabinoid Receptor-Gi Complex Structures. *Cell* **180**, 655-665 e618, doi:10.1016/j.cell.2020.01.008 (2020).

70 Kimura, K. T. *et al.* Structures of the 5-HT2A receptor in complex with the antipsychotics risperidone and zotepine. *Nat. Struct. Mol. Biol.* **26**, 121-128, doi:10.1038/s41594-018-0180-z (2019).

71 Peng, Y. *et al.* 5-HT2C Receptor Structures Reveal the Structural Basis of GPCR Polypharmacology. *Cell* **172**, 719-730 e714, doi:10.1016/j.cell.2018.01.001 (2018).

72 Liu, H. *et al.* Orthosteric and allosteric action of the C5a receptor antagonists. *Nat. Struct. Mol. Biol.* **25**, 472-481, doi:10.1038/s41594-018-0067-z (2018).

73 Wang, S. *et al.* Structure of the D2 dopamine receptor bound to the atypical antipsychotic drug risperidone. *Nature* **555**, 269-273, doi:10.1038/nature25758 (2018).

74 Schoppe, J. *et al.* Crystal structures of the human neurokinin 1 receptor in complex with clinically used antagonists. *Nat Commun* **10**, 17, doi:10.1038/s41467-018-07939-8 (2019).

75 Shiimura, Y. *et al.* Structure of an antagonist-bound ghrelin receptor reveals possible ghrelin recognition mode. *Nat Commun* **11**, 4160, doi:10.1038/s41467-020-17554-1 (2020).

76 Chen, X. *et al.* Molecular Mechanism for Ligand Recognition and Subtype Selectivity of alpha2C Adrenergic Receptor. *Cell reports* **29**, 2936-2943 e2934, doi:10.1016/j.celrep.2019.10.112 (2019).

77 Liu, K. *et al.* Structural basis of CXC chemokine receptor 2 activation and signalling. *Nature* **585**, 135-140, doi:10.1038/s41586-020-2492-5 (2020).

78 Vuckovic, Z. *et al.* Crystal structure of the M5 muscarinic acetylcholine receptor. *Proceedings of the National Academy of Sciences of the United States of America* **116**, 26001-26007, doi:10.1073/pnas.1914446116 (2019).

79 Ishchenko, A. *et al.* Toward G protein-coupled receptor structure-based drug design using X-ray lasers. *IUCrJ* **6**, 1106-1119, doi:10.1107/S2052252519013137 (2019).

80 Rappas, M. *et al.* Comparison of Orexin 1 and Orexin 2 Ligand Binding Modes Using X-ray Crystallography and Computational Analysis. *Journal of medicinal chemistry* **63**, 1528-1543, doi:10.1021/acs.jmedchem.9b01787 (2020).

81 Waltenspuhl, Y., Schoppe, J., Ehrenmann, J., Kummer, L. & Pluckthun, A. Crystal structure of the human oxytocin receptor. *Sci Adv* **6**, eabb5419, doi:10.1126/sciadv.abb5419 (2020).

82 Dal Maso, E. *et al.* The Molecular Control of Calcitonin Receptor Signaling. *ACS Pharmacol Transl Sci* **2**, 31-51, doi:10.1021/acsptsci.8b00056 (2019).

83 Liang, Y. L. *et al.* Structure and Dynamics of Adrenomedullin Receptors AM1 and AM2 Reveal Key Mechanisms in the Control of Receptor Phenotype by Receptor Activity-Modifying Proteins. *ACS Pharmacol Transl Sci* **3**, 263-284, doi:10.1021/acsptsci.9b00080 (2020).

84 Hollenstein, K. *et al.* Structure of class B GPCR corticotropin-releasing factor receptor 1. *Nature* **499**, 438-443, doi:10.1038/nature12357 (2013).

85 Dong, M. *et al.* Structure and dynamics of the active Gs-coupled human secretin receptor. *Nat Commun* **11**, 4137, doi:10.1038/s41467-020-17791-4 (2020).

86 Wang, J. *et al.* Cryo-EM structures of PAC1 receptor reveal ligand binding mechanism. *Cell Res.* **30**, 436-445, doi:10.1038/s41422-020-0280-2 (2020).

87 Duan, J. *et al.* Cryo-EM structure of an activated VIP1 receptor-G protein complex revealed by a NanoBiT tethering strategy. *Nat Commun* **11**, 4121, doi:10.1038/s41467-020-17933-8 (2020).

88 Jazayeri, A. *et al.* Extra-helical binding site of a glucagon receptor antagonist. *Nature* **533**, 274-277, doi:10.1038/nature17414 (2016).

89 Zhao, L. H. *et al.* Structure and dynamics of the active human parathyroid hormone receptor-1. *Science* **364**, 148-153, doi:10.1126/science.aav7942 (2019).

90 Wu, H. *et al.* Structure of a class C GPCR metabotropic glutamate receptor 1 bound to an allosteric modulator. *Science* **344**, 58-64, doi:10.1126/science.1249489 (2014).

91 Christopher, J. A. *et al.* Structure-Based Optimization Strategies for G Protein-Coupled Receptor (GPCR) Allosteric Modulators: A Case Study from Analyses of New Metabotropic Glutamate Receptor 5 (mGlu5) X-ray Structures. *Journal of medicinal chemistry* **62**, 207-222, doi:10.1021/acs.jmedchem.7b01722 (2019).

92 Yang, S. *et al.* Crystal structure of the Frizzled 4 receptor in a ligand-free state. *Nature* **560**, 666-670, doi:10.1038/s41586-018-0447-x (2018).

93 Tsutsumi, N. *et al.* Structure of human Frizzled5 by fiducial-assisted cryo-EM supports a heterodimeric mechanism of canonical Wnt signaling. *Elife* **9**, doi:10.7554/eLife.58464 (2020).

94 Burley, S. K. *et al.* RCSB Protein Data Bank: biological macromolecular structures enabling research and education in fundamental biology, biomedicine, biotechnology and energy. *Nucleic Acids Res.* **47**, D464-D474, doi:10.1093/nar/gky1004 (2019).

95 Armstrong, D. R. *et al.* PDBe: improved findability of macromolecular structure data in the PDB. *Nucleic Acids Res.* **48**, D335-D343, doi:10.1093/nar/gkz990 (2020).

96 Kooistra, A. J., Munk, C., Hauser, A. S. & Gloriam, D. E. An online resource for comparative GPCR structure analysis. *Submitted*.

Figures

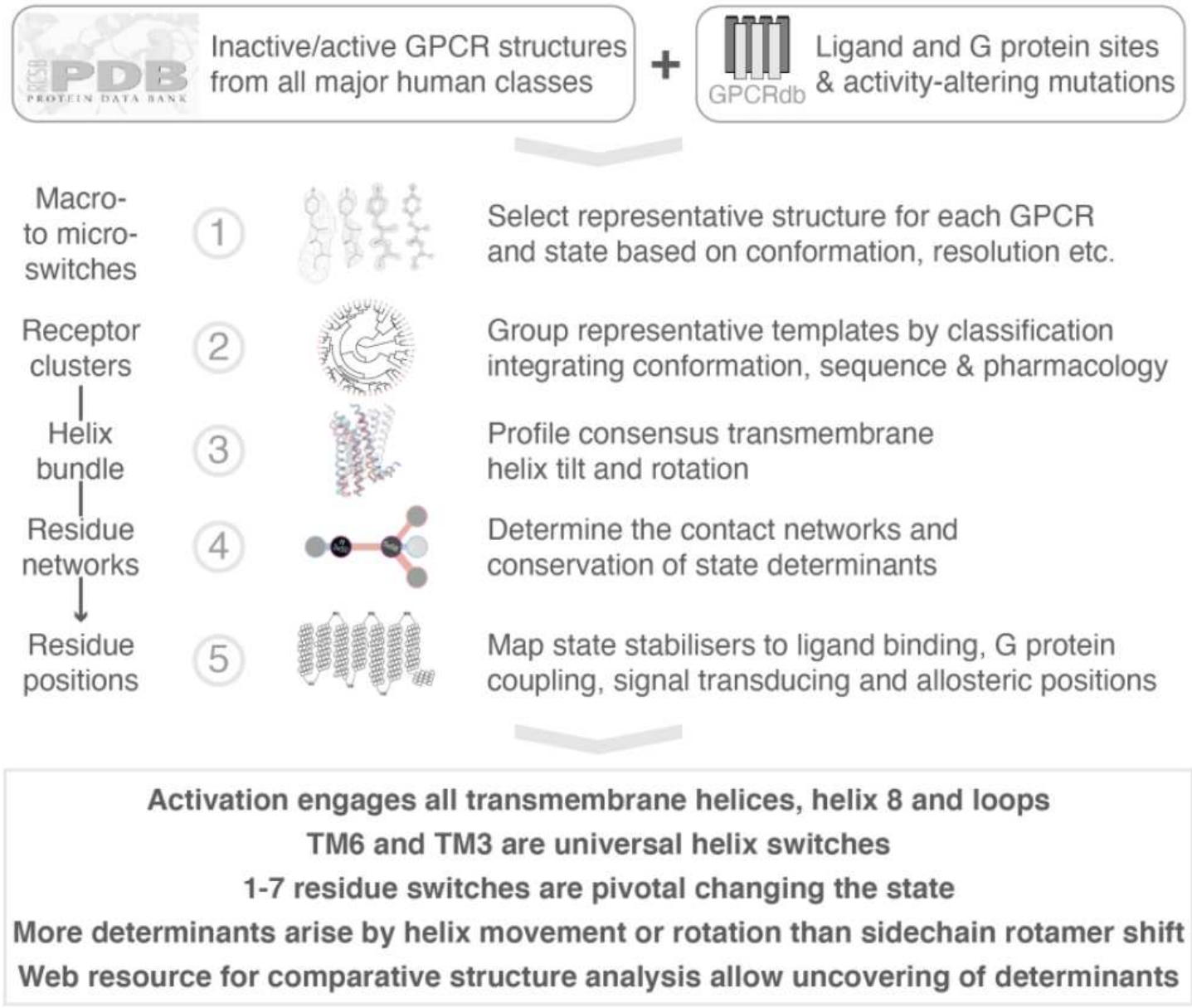

Figure 1

Analysis pipeline for elucidation of GPCR activation mechanisms. Pipeline for analysis of universal and distinct activation macro-/microswitches spanning helix repacking to sidechain rotation and connection to ligand binding, G protein coupling and signal transduction sites (see Methods).

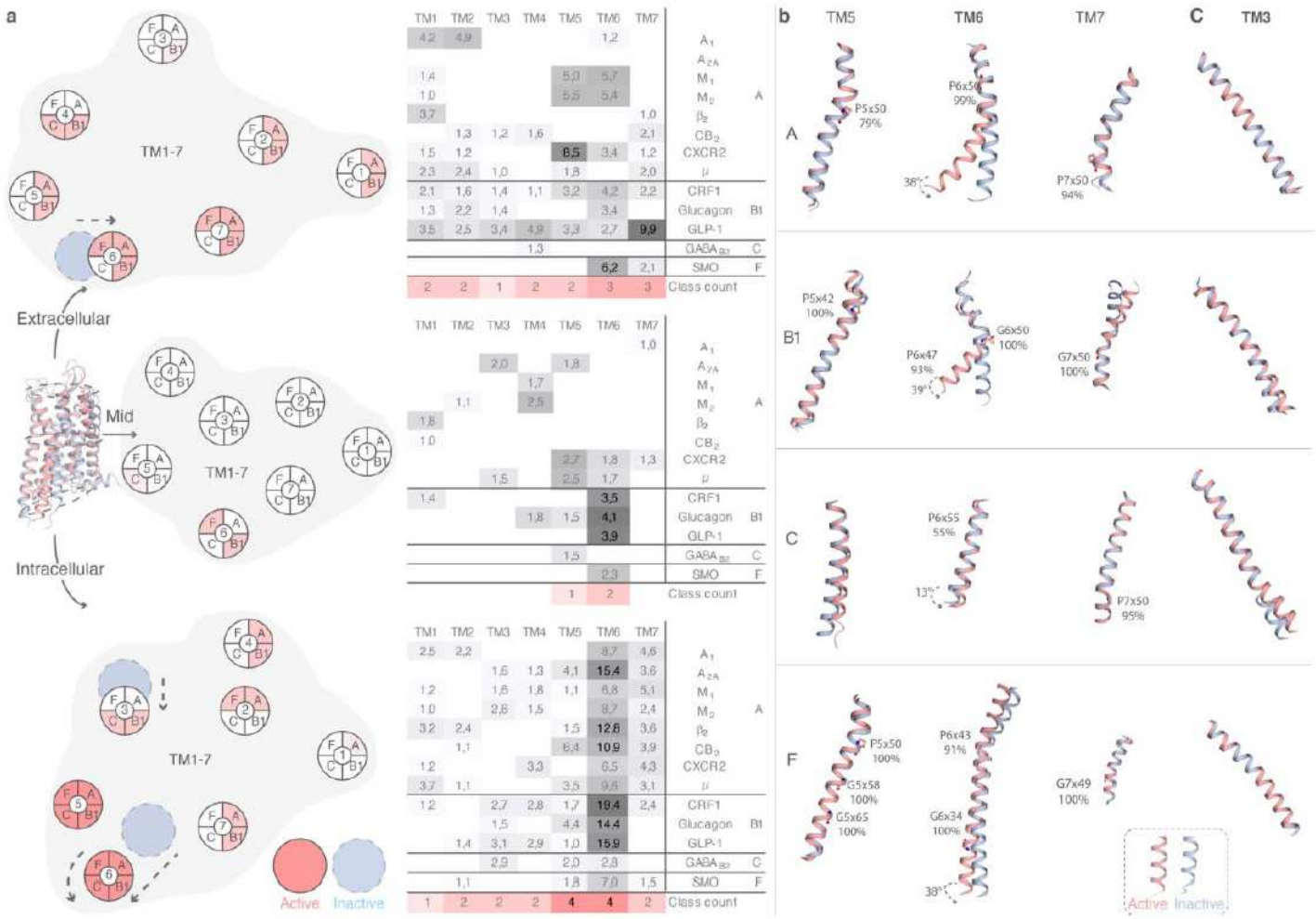

Figure 2

Transmembrane helix movement upon activation and universal TM3 and TM6 helix ‘macroswitches’. a, Movements (Å) over 1.0 Å at the extracellular end, membrane mid (determined using35) and intracellular end of the transmembrane helices, TM1-7 upon comparison of all available receptor inactive- and active-state structure pairs (Extended Data Table 1). Red intensity denotes the number of classes with a consensus movement (for class C, priority is given to the Gi-GABAB2 over the non-coupled mGluR5 structure). b, Movement and conserved hinges of TM6 and the adjacent TM5 and TM7. c, TM3 cytosolic tilt and overall rotation. b-c, GPCR class representative inactive/active receptor structure pairs: A: β236,37, B1: GLP-118,22, C: GABAB238 and F: Smoothened39,40 receptors. Proline and glycine residues that increase helix plasticity are shown along with their percent conservation in the GPCR class.

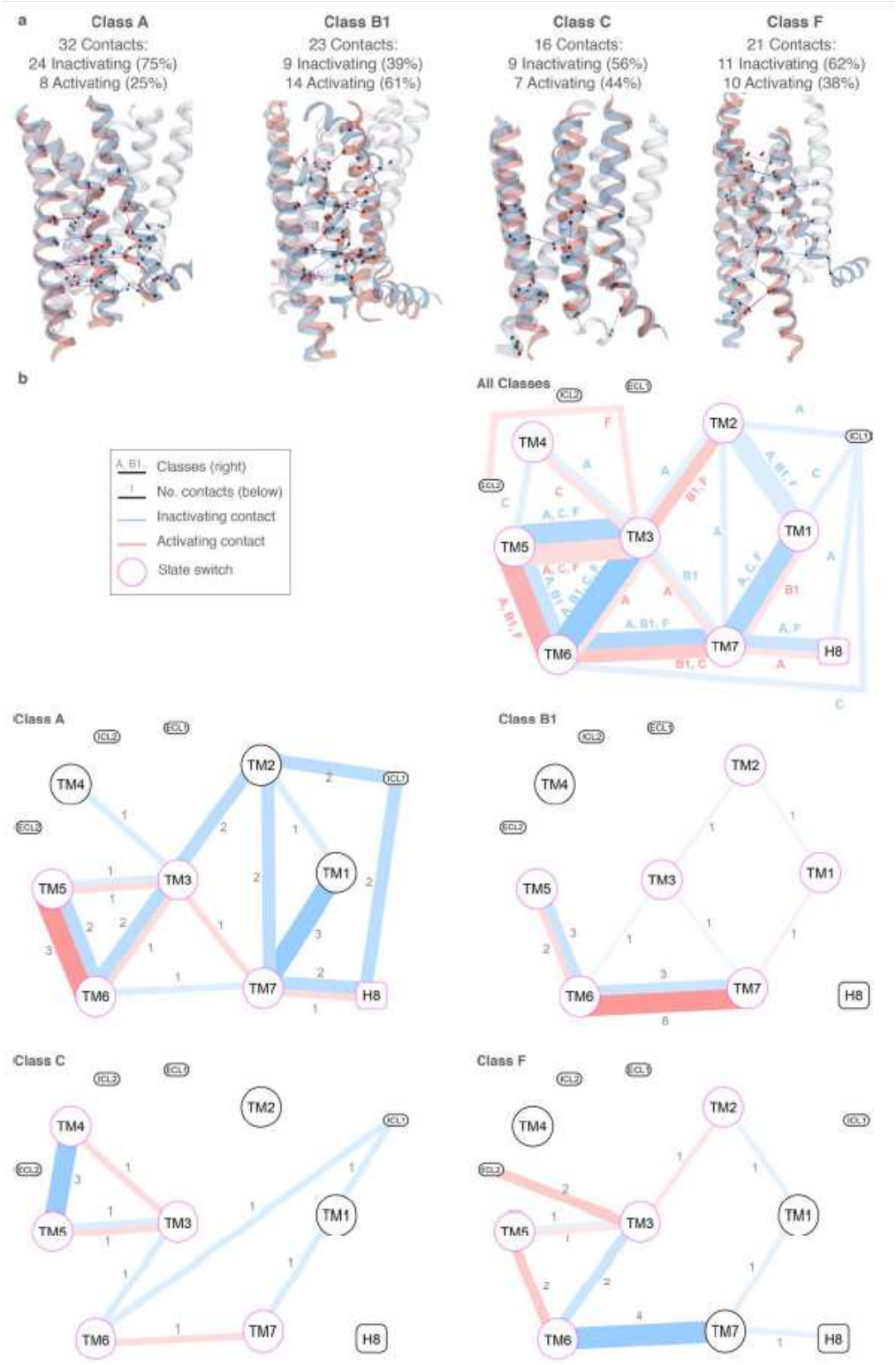

Figure 3

GPCR stabilise inactive and active states by rerouting contacts between TM1-7, H8, ICL1 and ECL2. a, State-specific residue-residue contacts in each GPCR class visualised as lines within representative inactive/active receptor structure pairs (same as in Fig. 2b-c). Numbers indicate the total, inactivating and activating contacts in each GPCR class. b, Contact networks between the seven GPCR transmembrane helices, TM1-7 and the first intracellular (ICL1) and second extracellular (ECL2) loops (intra-segment

contacts not shown). Line thickness represents the number of classes (topmost) or contact frequency differences between the inactive and active states. Line colour indicates inactivating (blue) and activating (red) contacts. Receptor segments with a magenta border are “switches”, i.e. have contacts across both states. Contacts are identified based on a higher frequency (%) in one set of 43 inactive and 25 active state receptors. a-b, The frequency difference thresholds was set according to the structural coverage in each GPCR class’ (no. members and inactive/active state templates): A: 40% (285, 33/14), B1: 67% (15, 3/10), C: 75% (22, 4/1) and F: 100% (11, 3/1) – yielding comparable numbers of determinants and contacts. To ensure that the identified determinants are applicable for throughout each class, we applied a cut-off requiring at least 30% of all its receptors to contain one of the amino acid pairs observed to form the given state specific contact. Contact definitions are explained in the settings menu of the online ‘Comparative structure analysis’ tool (https://review.gpcrdb.org/structure_comparison/comparative_analysis).

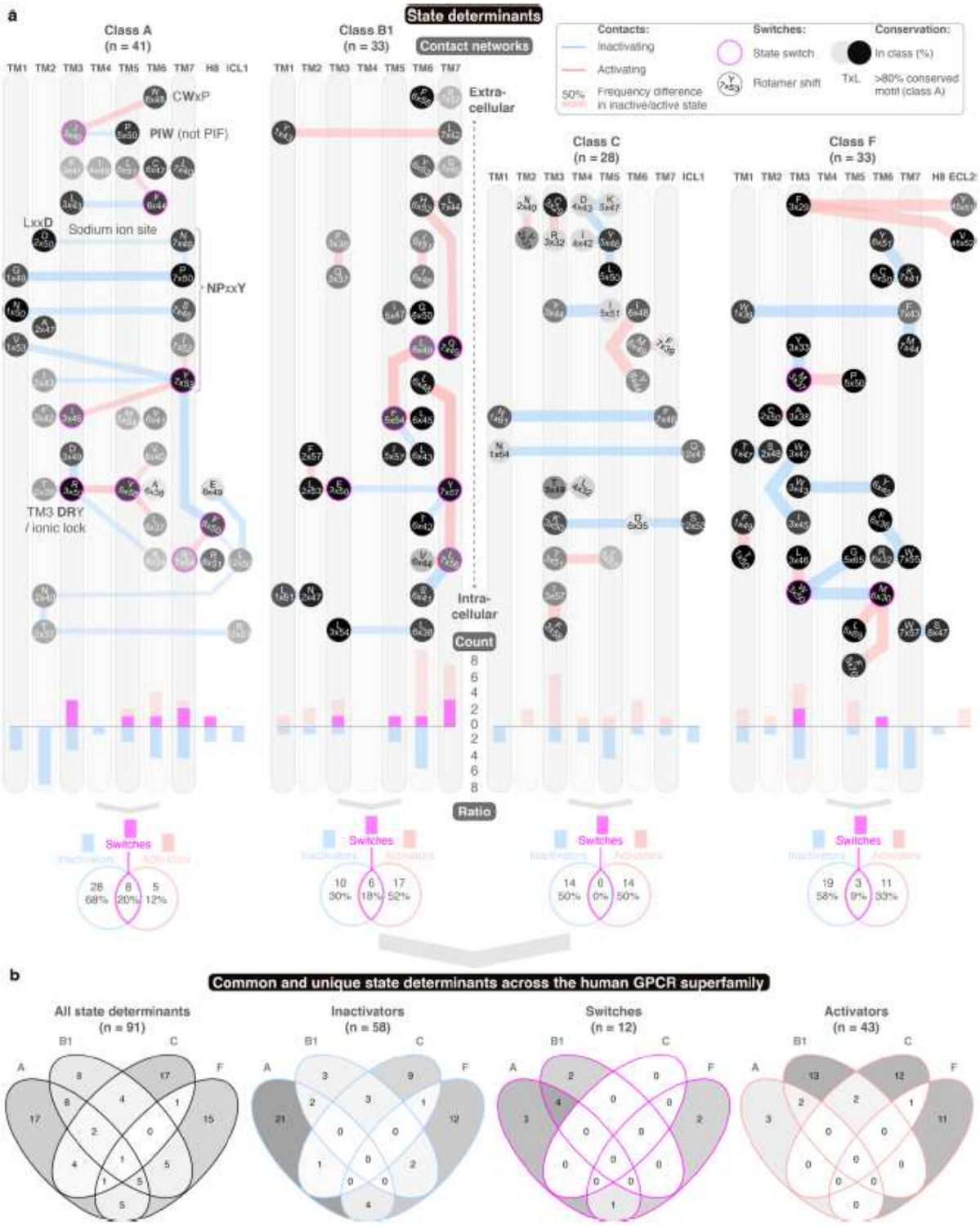

Figure 4

State stabilising contact maps and differences at the residue-level ‘microswitches’. a, Contact networks visualise the wiring of state determinants from the extracellular (top) to intracellular (bottom) sides. Contact frequency differences between the inactive and active states are shown as varied line thickness and residue rotamers as rotation of the consensus amino acid in analysed structures and its generic residue number. Two-way Venn diagrams depict the number and percentages of inactivator (blue),

activator (red) and switch (magenta) state determinant positions. Bar diagrams show their distribution across the TM helices, H8 and loops. b, Comparison of common and unique state determinant positions across all investigated classes.

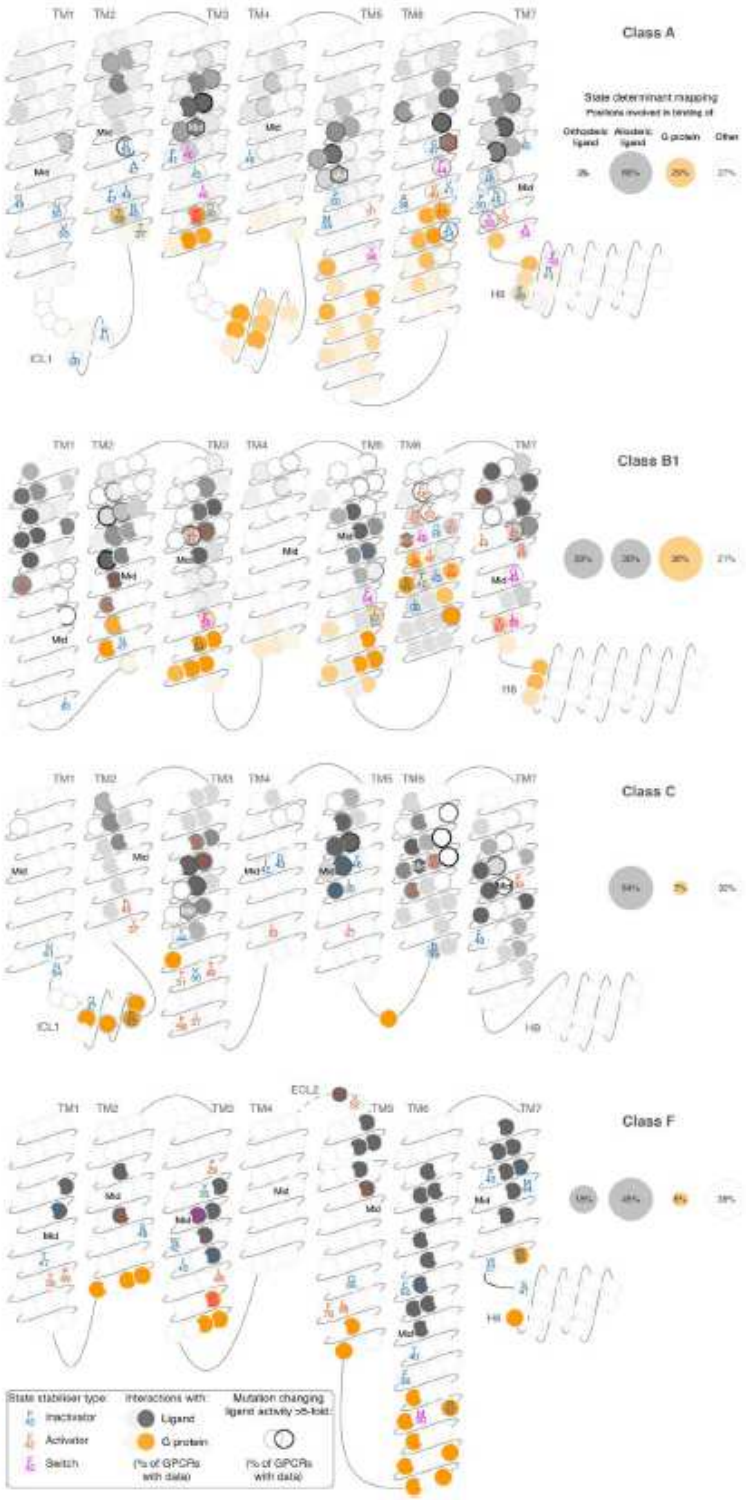

Figure 5

Residue positions stabilising an inactive and/or active receptor state. GPCR snakeplots mapping the residue positions that form distinct contacts between state determinants classified as inactivators (blue),

activators (red) and switches (magenta). Residues are denoted with the consensus amino acid of the investigated receptor structures (Extended Data Table 1) and their generic residue number26. Filled positions map ligand (grey) and G protein (orange) interaction frequency among all GPCRs in the given class that have such data (Supplementary Spreadsheet 2). Border grayscale denotes the frequency of mutations changing the ligand affinity or activity over 5-fold. The label “Mid” within hexagon-shaped positions denote the membrane mid, above and below which the ligand positions are considered orthosteric and allosteric, respectively, in class A, B1 and F. In class C, all ligand interacting positions in the seven transmembrane helices are allosteric, as its endogenous ligands bind solely in the N-terminal domain.